EUROPEAN ORGANIZATION FOR NUCLEAR RESEARCH

CERN/EP/85-103
27 June 1985

CHARM HADRON PROPERTIES IN 360 GeV/c π^-P-INTERACTIONS

LEBC-EHS COLLABORATION

M. Aguilar-Benitez[9], W.W.M.Allison[11], J.F. Baland[10], S. Banerjee[2], W. Bartl[23], M. Begalli[1], P. Belliere[5], A. Bettini[12], L. de Billy[13], R. Bizarri[14], G. Borreani[21], H. Briand[13], R. Brun[4], W.M. Bugg[20], E. di Capua[14], C. Caso[6], B. Castano[9], E. Castelli[22], P. Checchia[12], P. Chliapnikov[17], S. Colwill[11], R. Contri[6], D. Crennel[15], M. Cresti[12], A. De-Angelis[12], C. Defoix[5], R. Dimarco[16], J. Dolbeau[5], J. Dumarchez[13], B. Epp[23], S. Falciano[14], C. Fernandez[4], C. Fisher[15], Yu. Fisyak[17], F. Fontanelli[6], J.R. Fry[8], S. Ganguli[2], L. Garbellini[21], U. Gasparini[12], S. Gentile[14], A. Goshaw[4], F. Grard[10], A. Gurtu[4], R. Hamatsu[7], T. Handler[20], E.L. Hart[20], L. Haupt[18], S. Hellman[18], J.J. Hernandez[4], A. Herve[4], S.O. Holmgren[18], M.A. Houlden[8], J. Hrubec[23], P. Hughes[15], D. Huss[19], Y. Iga[7], M. Iori[4], E. Jegham[19], E. Johanson[18], J. Kesteman[10], E. Kistenev[17], I. Kita[7], S. Kitamura[7], V. Kniazev[17], P. Ladron de Guevara[9], M. Laloum[5], J. Lemonne[3], H. Leutz[4], L. Lyons[11], M. MacDermott[15], P.K. Malhotra[2], F. Marchetto[21], G. Marel[14], F. Marzano[14], P. Mason[8], M. Mazzucato[12], A. Michalon[19], M.E. Michalon-Mentzer[19], T. Moa[18], R. Monge[6], L. Montanet[4], G. Neuhofer[4], H.K. Nguyen[13], S. Nilsson[18], H. Nowak[4], N. Oshima[7], G. Otter[1], G.D. Patel[8], M. Pernicka[23], P. Pilette[10], C. Pinori[12], G. Piredda[14], R. Plano[16], A. Poppleton[4], P. Poropat[22], B. Powell[4], G. Ransone[1], S. Reucroft[4], J. Richardson[4], G. Rinaudo[21], K. Roberts[8], H. Rohringer[23], M. Schouten[4], R. Schulte[1], B. Sellden[18], M. Sessa[22], K. Shankar[2], S. Squarcia[6], P. Stamer[16], V. Stopchenko[17], W. Struczinski[1], A. Subramanian[2], M.C. Touboul[13], U. Trevisan[6], C. Troncon[22], T. Tsurugai[7], V. Uvarov[17], L. Ventura[12], P. Vilain[3], E. Vlasov[17], C. Voltolini[19], B. Vonck[3], J. Wickens[3], C. Willmott[9], P. Wright[11], T. Yamagata[7], V. Yarba[17], L. Zanello[14], P.L. Zotto[12] and G. Zumerle[12]

(submitted to Zeitschrift für Physik)

---

[1]Aachen, [2]Bombay, [3]Brussels, [4]CERN, [5]College de France, [6]Genova, [7]Japan Universities, [8]Liverpool, [9]Madrid, [10]Mons, [11]Oxford, [12]Padova, [13]Paris, [14]Rome, [15]Rutherford Lab, [16]Rutgers, [17]Serpukhov, [18]Stockholm, [19]Strasbourg, [20]Tennessee, [21]Torino, [22]Trieste and [23]Vienna

ABSTRACT

We report results on hadrons with open charm quantum number from 360 GeV/c π^-p interactions. The total charm cross-section for $x_F > 0$ is found to be 20.2±4.8 μb, consisting of 10.1±2.2 μb for D^0 and $\bar{D}^0$, 5.7±1.5 μb for $D^{\pm}$ and 4.5±4 μb for Λ_c. We observe no unambiguous F-meson and derive an upper limit for F-production for $x_F > 0$ as a function of $\tau(F)$. D* production accounts for all of the $D^0/\bar{D}^0$ production, and 48±27% of the production of $D^{\pm}$. The lifetimes from kinematically fitted events are: $3.5^{+1.4}_{-0.9} * 10^{-13}$ s for neutral D-mesons, $9.8^{+3.4}_{-2.2} * 10^{-13}$ s for charged D-mesons. The average of the proper time, corrected for short distance losses, for three unique Λ_c is $0.4 * 10^{-13}$ s. The best fit for the x_F distribution for D-mesons is achieved for n = 3.8 if described by $d\sigma/dx_F \alpha (1-x_F)^n$. A strong effect of leading quarks is found. A better fit is achieved if we assume a fraction α proportional to $(1-x_F)^m$ and $(1-\alpha)$ proportional to $(1-x_F)^n$, for which the best fit is α = 0.80, m = 7.5 and n = 0.7. For D*-mesons the best fit is obtained for $n = 4.3^{+1.8}_{-1.5}$. The p_t distribution of D-mesons is described by $d\sigma/dp_t^2 \alpha \exp(-bp_t^2)$, with $b = 1.0 \pm 0.1$ $(GeV/c)^{-2}$. For the p_t distribution of D*-mesons the best fit is $b = 0.9^{+0.4}_{-0.3}$ $(GeV/c)^{-2}$.

1. INTRODUCTION

Data on hadroproduction of charm particles are still scarce and incomplete. Experiments in general suffer from the uncertainties in the branching ratios to the observed final states, in the A dependence of the cross section, in the correlations between members of the charm pair and in the constraints due to the limited phase space for both the trigger and detection. Such effects can severely limit the validity of the conclusions concerning production properties. In the experiment presented here these difficulties have been greatly reduced by the use of the high resolution hydrogen bubble chamber LEBC (LExan Bubble Chamber) which allowed the detection with high efficiency of the charm particles produced in "visible" hydrogen interactions and leading to "visible" decays, free from topological ambiguities. The limitation is the low sensitivity of a bubble chamber experiment, typically a few events per microbarn. The statistical errors dominate the possible systematic errors. The results described were obtained by the CERN experiment NA27 from an exposure of LEBC and the European Hybrid Spectrometer (EHS) to a 360 GeV/c π^- beam from the CERN SPS. Preliminary results [1] and partial results based on a subsample of our neutral decays [2] have been presented elsewhere.

2 EXPERIMENTAL SET-UP

The experimental set-up is shown in fig 1. A preliminary version of the EHS-spectrometer, used for the experiment NA16 has been extensively described elsewhere [3]. The major improvements are the new bubble chamber LEBC 2, the improved particle identification by ISIS 2 and the new trigger. Detector dimensions are given as (horizontal) x (vertical), positions are given with reference to the centre of LEBC.

2.1 The Beam

The H2 beam [4] had a focus at LEBC in the horizontal plane with full width (at base) of $\simeq$ 2 mm. This focus coincided with the depth of focus

of the LEBC optical system. In the vertical plane the beam was slightly divergent (±0.1 mrad) and 3 cm wide. The beam momentum was 360 GeV/c with a momentum byte $\Delta p/p < 1\%$. The total flux was typically $\simeq 5 \times 10^4$ π^- during the $\simeq$ 2 s spill every $\simeq$ 12 s. Contamination from $\bar{p}$ and μ^- is estimated to be $<< 1\%$. In order to minimise the space charge effect in ISIS the beam was equipped with a rotating collimator, placed upstream of target T2, to interrupt the incident 400 GeV/c protons. This collimator let through particles for $\simeq$ 2 ms every $\simeq$ 30 ms. Each LEBC pressure minimum was synchronised with, and centered on, each $\simeq$ 2 ms quasi-spill. In addition to the rotating collimator, the beam was also equipped with a fast kicker system [5] upstream of target T2, which deflected the incident protons off target, thus giving no secondary particles during the kick. The beam was kicked out just before the LEBC sensitive time and after an interaction trigger was accepted. The combination of kicker and rotating collimator reduced the total spill flux to $\simeq$ 1000 beam particles concentrated in approximately 60 spikes of < 500 μs duration.

2.2 The LEBC Bubble Chamber

LEBC is a rapid cycling (30 Hz) hydrogen bubble chamber. A spatial (two track) resolution of about 20 μm is necessary to be sensitive to lifetimes as short as 10^{-13} s. This requires high resolution optics and expansion cycles nearly down to the foam limit of hydrogen to achieve high bubble density along the particle tracks. Therefore LEBC was constructed as a "clean bubble chamber" without any seals, or other parts which could favour parasitic boiling [6]. The chamber body (fig. 2) is built entirely from LEXAN(*) a thermoplastic polycarbonate, which is transparent for visible light and exhibits an extraordinarily high impact strength even at cryogenic temperatures. To achieve highest possible resolution, LEBC 2 was designed with two optics windows for straight-through illumination. The photographed chamber volume has dimensions of 12 cm along the beam, 7 cm deep, on axis with the optics and visible height of $\simeq$ 5 cm to match the 5 cm film width at 1:1 demagnification. The flash for picture taking was

---

(*) "Press-polished" optical grade LEXAN from Westlake Plastics Company, Lenni, Pennsylvania (USA)

activated by an interaction trigger. Two Xenon flash-tubes illuminated, via a condensor lens (fig. 3) the chamber volume. Each light beam was focused into the centre of its corresponding camera objective, where its aperture was adjusted to subtend symmetrically the central (first order) cone of the diffraction pattern. At our bubble sizes, the diffracted intensity exceeds the refracted intensity by nearly two orders of magnitude. The pictures were taken in bright field illumination, which again requires less light than dark field photography. The illuminating light passes through the centre of the objective lens and blackens the film over the entire picture area except where it interferes with the diffraction cone from a bubble to leave the unexposed image of the bubble. This application of diffractive bright field photography is the only means of rendering our small bubbles visible on film. A typical quality photograph is shown in fig. 4. The chamber conditions during picture taking are listed in table 1.

TABLE 1

LEBC operating conditions and optics parameters

Hydrogen temperature	29.1 K	
Hydrogen static pressure	8.3 bar	
Expansion pressure minimum	3.9 bar	
Piston stroke	0.5 mm	
Duration of expansion cycle	6 ms	
Beam gate at pressure minimum	500 μs	
Expansion cycling rate	30 Hz	
Camera cycling rate	15 Hz	
Bubble density along tracks	80 cm^{-1}	
Objective	Schneider Componon S	
Focal length	350 mm	
Demagnification	1:1	
Stereo angle	13°	
Lens apertures (view 1 and view 2)	F/13	F/16
Nominal depth of field	1.5 mm	2.0 mm
Bubble growth time (flash delay)	70 μs	120 μs
Bubble diameter	17 μm	22 μm

2.3 The EHS Spectrometer

Magnets

Two magnets, M1 and M2, were used to provide momentum analysis. M1, situated 2.7 m downstream of LEBC, is a superconducting stretched Helmholtz-coil magnet, with horizontal aperture of 80 cm. The central field was chosen at 1.1 T, giving an integrated field of 2.1 Tm, corresponding to a transverse momentum kick of 620 MeV/c. M2, situated 20 m downstream of LEBC, is a conventional U-magnet with aperture 40x100 cm^2. The central field used was $\simeq$ 1.3 T, giving an integrated field of 3.1 Tm, which corresponds to a momentum kick of 950 MeV/c.

Drift and Wire Chambers

The drift chambers had a sensitive surface of 2x4 m^2 (D1-D3) and 1.3x2 m^2 (D4-D6) respectively [3,7] see fig. 1. The space point precision obtained in this part of the experiment was $\simeq$ 300 μm in the bending plane and 1.5 mm in the non bending plane.

The two multiwire proportional chambers W0 and W1 were placed immediately downstream of LEBC, at 33 and 87 cm respectively. Both chambers consisted of one plane with vertical wires. W0 is a 500 μm pitch chamber with 160 wires and a sensitive area of 8x10 cm^2, [8]. W1 is a 1 mm pitch chamber with 320 wires and a sensitive area of 32x32 cm^2, which is a scaled-down version of the design described in [9]. The chambers were equipped with a fast read-out of the anode wires, and were used both for track reconstruction and to form the interaction trigger.

The large MWPC W2 was placed 4.2 m downstream of the centre of LEBC. This chamber has a sensitive area of 1.2x2.15 m^2 and six 2 mm pitch coordinate planes.

The Proportional Inclined Chamber - PIC [10], used for tracking, was situated at the center of the magnet M1, and was inclined 35° with respect to the vertical. The two planes, 13 cm apart each had 640 wires, with drift time read-out, spaced at 2 mm with an angle of $\simeq$ 10° with respect to the horizontal. The sensitive detector area was 50x128 cm^2. With the magnetic field on, the spatial resolution for each plane was 90 μm for clean beam tracks, and for outgoing secondary tracks better than 200 μm. The two track separation limit was $\simeq$500 μm.

The Silica Aerogel Detector

The Silica Aerogel Cherenkov Detector (SAD) [11] was situated 5 m downstream of LEBC, close to the magnet M1. It is composed of 18 identical modules, each one having a sensitive surface of 23x55 cm^2 resulting in a total detector surface of 2.3 m^2. The threshold momentum is 0.56 GeV/c for π, 2.0 GeV/c for K and 3.8 GeV/c for protons. SAD is useful for particle identification in the momentum range 0.6-4.5 GeV/c. The reliability of the identification has been checked using kinematically fitted neutral particles (γ, K^0, Λ^0) and charged particles identified by ISIS.

ISIS

The large pictorial drift chamber ISIS 2 (the acronym stands for Identification of Secondaries by Ionisation Sampling) had its center 10 m downstream of LEBC. It is equipped with 320 wires transverse to the beam, in a horizontal plane. Its fiducial volume is 4 m height, 2 m width and 5 m length. ISIS fulfilled two functions in EHS; the first was to produce high quality track vectors which were used to initialise track reconstruction in the spectrometer; the second was to measure, by dE/dX, the velocity of each track so that when the momentum was also known, the particle mass might be deduced. The technique, which relies on the relativistic increase of the ionisation in a gas, has been extensively reviewed [12,13], and the successful application in ISIS 2 has been described elsewhere [14]. Briefly the ionisation resolution achieved is close to the theoretical performance and the particle identification has been checked by examining a large sample of tracks from reconstructed K^0 and Λ^0 decays and γ conversions observed in the bubble chamber during the course of this experiment. We found that electrons are uniquely resolved at the 1% level (as defined in [13]) for momenta range below 20 GeV/c, whereas for K/π separation the range is 3-30 GeV/c.

Gamma Detectors

Photons and electrons were detected by the two lead glass calorimeters, the Intermediate Gamma Detector (IGD), and the Forward Gamma Detector (FGD) [3,15]. The IGD, placed 17 m downstream of LEBC, is an array of 1122 lead glass blocks with a cross section of 5x5 cm^2 and length corresponding to 15 radiation lengths. The detector surface is 195x160 cm^2, with a central aperture of 35x90 cm^2, matching the gap in the M2 magnet. The IGD has an energy resolution (FWHM) $\Delta E/E=(15/\sqrt{E+2})\%$, with E

in GeV. Spatially it is possible to resolve two showers of equal energy down to a separation of 25 mm, at a 95% confidence level.

The FGD, situated 42 m downstream of LEBC, is longitudinally segmented into a converter wall of 5 radiation lengths, a finger hodoscope for determining shower location and an absorber wall with length varying between 16 and 24 radiation lengths. The detector surface of 120x210 cm^2, covers the image of the hole in IGD. The energy resolution for FGD (FWHM) is $\Delta E/E=(10/\sqrt{E}+2)\%$, with E in GeV. In FGD two separate showers are recognised as such if their separation is larger than 30 mm, which allows us to separate the two gammas from π^0 of momenta up to 300 GeV/c (95% C.L.). The width of the π^0-mass peak is $\simeq$ 20 MeV/c^2 for both detectors.

2.4 Over-all Performances

For charged tracks LEBC provides topological information and space angles with a precision of 0.2 mrad in the bending plane and 2.0 mrad in the non-bending plane. Forward tracks with an angle of less than 100 mrad to the beam axis are within the spectrometer acceptance. The frame of PIC and the aperture of the M1 magnet limit the analysis to tracks within 100 mrad of the beam in the non-bending plane. Tracks in the 100-200 mrad range in the bending plane are found with reduced efficiency. All tracks in the forward hemisphere ($x_F > 0$), and about 25% of tracks at negative x_F are within the spectrometer acceptance. Track precision below 50 GeV/c momentum is limited by multiple Coulomb scattering to $\Delta p/p \simeq 0.5\%$. For tracks traversing the second magnet the additional momentum analysis provided ensures $\Delta p/p < 0.5\%$ up to 120 GeV/c. Angle measurements are again limited by multiple scattering and are typically in the range 0.1-1.0 mrad for particles coming from charm decays. For all charged particle final states the effective mass resolution is in the range 4-8 MeV/c^2 at the D-mass. For D decays including an additional π^0 reconstructed from the gamma detectors, the effective mass resolution is $\simeq$ 15 MeV/c^2.

2.5 The Trigger

The decision to flash the bubble chamber illumination and to read out the spectrometer was taken by a "minimum bias" trigger. To define an interaction,the trigger required more than two hits in each of the two wire

chambers W0 and W1. Figure 5 shows the charged primary multiplicity distribution observed in LEBC for all events together with measured multiplicity distributions for 360 GeV/c π^-p from [16]. The distributions have been normalised to each other for $n_{charged} \geq 10$. Table 2 shows the trigger efficiencies for different charged multiplicities(*).

Table 2

Trigger efficiency for low multiplicities.

Multiplicity	Trigger efficiency (%)
2 (inelastic)	19 ± 2
4	43 ± 2
6	68 ± 3
8	87 ± 3

Folding these efficiencies with the distribution of charged tracks for the charm events, including also the charged decay products, we have computed the trigger efficiency for charm-events to be 98^{+2}_{-3} %. The trigger rate, defined as the number of triggers per incoming beam, was $1.4 * 10^{-2}$. This rate was continously checked for stability during data taking.

3. DATA REDUCTION AND ANALYSIS

3.1 Data Conventions

In what follows we use the NA27 conventions and label the decays Cn or Vn respectively, C for a charged decay, V for a neutral decay and n for the number of charged decay products. For each charged decay product track, we

(*) The contribution from two-prongs is explained by knock off electrons, particles firing more than one wire etc.

define the "impact parameter", y, at the primary vertex, $y = L\sin\phi$ (fig. 6a). For an interaction with one or several associated decays, the largest of the impact parameters, y_M is a good measure of the visibility, hence we normally impose a cut on this parameter to ensure high detection efficiency. The smallest impact parameter, y_m, gives a measure of the clarity of the topology and a cut on this quantity is used to guarantee an unambiguous topology.

3.2 The Sample

265 000 bubble chamber pictures contained a primary hydrogen interaction in the fiducial volume, 8.5 cm along the beam, ≃ 5cm wide. These events correspond to a triggered inelastic cross section of 16.8 mb, giving a total sensitivity of 15.8 ± 0.8 events per μb. Of these 265000 pictures, 6368 had a secondary decay fulfilling the criteria for potential charm candidates described in section 3.3 and were subsequently measured. After this measurement a first geometrical reconstruction and kinematical analysis was performed yielding 276 events containing candidates for charm. In this first reduction, decays were eliminated as being strange particle decays or gamma conversions. The 276 events with charm candidates were remeasured on the Strasbourg HPD, see section 3.4. The complete analysis reduced the sample to 116 events containing 183 charm decays.

3.3 Scanning

The charmed particles are detected by observing their decay in the bubble chamber. A "scan box" was defined as a rectangle on the LEBC picture with a width of 4 mm centered on the interacting beam track and a length extending through the whole bubble chamber. Confining the scanning to this box effectively reduces the background from strange particles without affecting the charm sample, since $|L \sin\theta| = Lp_t/p = p_t ct/m = O(ct)$ (fig. 6b). For $t < 10^{-12}$ s, $|L \sin\theta| \lesssim 0.3$ mm, so the cut has little effect on charm-decays. This is supported by the distribution of $|L \sin\theta|$ of our charm candidates (fig. 7) which peaks strongly at zero and has no entry for $|L \sin\theta| > 0.8$ mm. Each frame was scanned twice on two views and with two different magnifications (≃ 10x and ≃ 30x). For each frame the prediction for the transverse position of the interacting beam particle was provided from information in wire-chambers upstream of

the experiment. If a primary interaction matching the prediction was found inside the fiducial volume, the event was scanned for secondary activity (interactions, decays, tracks not coming from the primary vertex and also sudden jumps in ionisation) inside the "scan box". Finally a check scan was made by a physicist. The double scanning efficiency is 98% for charged secondary interactions and neutral strange particle decays, and 90% for charged strange particle decays. However, one cannot infer the charmed particle scanning efficiency from the strange particle ones, since their decay length distribution is considerably shorter, their topology distribution is different (for strange decays the C1 and V2 topologies dominate, while for charmed decays the number of decays into C1/C3 and V2/V4 topologies respectively are roughly similar). Also the charm decays are scrutinized several times on devices with considerably better resolution than for scanning, and thus the detection of one charm decay often leads to the detection of its partner at a later stage. The combined efficiency to detect a charm decay in the scanning - check scanning - measurement - remeasurement process is estimated at 85-95 ± 5%, depending on decay topology and the cuts applied. For the sample used in the cross section calculations the efficiency is 95 ± 5% for the V4 and C3 topologies and 90 ± 5% for the V2 topology.

3.4 Measuring reconstruction and kinematics:

All events with decays found in the scan box were measured. Those having a decay in the charm box (defined as a cylinder in space, centered on the incoming beam track, with a radius of 1 mm for C1 and V2 topologies and 2 mm for the other topologies) were remeasured on the high precision measuring machine (HPD) in Strasbourg if satisfying one of the following conditions:

- A C1 or V2 topology where one of the decay products had a transverse momentum relative to the line of flight of the parent particle larger than 250 MeV/c. This cut is designed to remove strange particle decays. A Monte Carlo simulation of the charm particle decays show that this cut removes only about 4% of the charm signal in these topologies.
- A "topological charm" i.e. C3, C5, V4 or V6;
- All unclear topologies, i.e. events with a confused secondary vertex.

The whole charm sample was remeasured on the HPD to homogenize the measurements for the final charm sample and to have a good control of resolution and measurement errors. The Strasbourg HPD [17] combined with graphical facilities is the device in the collaboration that has the highest precision and resolution. During the measurement procedure, the event is projected onto the scanning table, and the HPD digitisations are displayed on the interactive screen. Zooming, rotating and using the different magnifications in X and Y is a very powerful tool for localising and measuring accurately the kinks and vertices. Fig. 8 shows a digitization of the event shown in fig. 4. Using this procedure the distribution of residuals of the master points has an RMS of 1.8 μm on the film, and, if the track environment is favourable, the detection of impact parameters down to 7 μm on film is possible. These characteristics make the HPD an excellent device to measure charm events and to clarify difficult topologies. In this process charm particle decays undetectable at scanning were discovered; in 116 events remeasured on the HPD and subsequently classified as charm 27 previously unseen decays were found. These numbers are fully compatible with the visibility weights described in section 3.5.

Geometrical Reconstruction

The 2-dimensional track elements provided by ISIS were used to initiate the geometrical reconstruction. Combining these with hits in the surrounding chambers it was possible to construct track elements in space. These were extrapolated through the M1 magnetic field and associated to tracks measured in LEBC according to their projected angles. By this stage 90% of the tracks seen in LEBC inside the angular acceptance of the spectrometer were reconstructed. Analysis of K^0 and Λ^0 decays showed incorrect associations to occur for less than 1% of these tracks. Bubble chamber tracks not found in the spectrometer were combined with unused hits in the detectors upstream of ISIS to recover low momentum particles or to localize secondary interactions in the spectrometer. For this category of tracks the contamination from incorrect associations was somewhat larger. In these cases the geometrical reconstruction was improved with the use of an interactive graphical system with which it was possible to display an event in the whole EHS, or any part of it, showing both geometrically fitted tracks and information from the detectors. It was also possible to change the track parameters on-line to observe the changes in the

trajectories as the particles traverses the EHS spectrometer. Using this system every track from a charm candidate was scrutinised to identify incorrect track associations, particularily focusing on tracks which used few hits in the spectrometer, tracks which had primary tracks close-by in angle and space (this was the most common source of incorrect associations between spectrometer tracks and tracks seen in the bubble chamber) and tracks for which the geometry program could not find an expected ISIS track segment. After this process the level of incorrect associations between spectrometer- and bubble chamber tracks is negligble. All pair combinations of spectrometer track elements not associated with bubble chamber tracks were analysed to reconstruct γ conversions and neutral strange particle decays downstream of LEBC. The efficiency for finding this type of particles, when tested on tracks coming from strange particle decays seen in the bubble chamber (not using the bubble chamber information), was found to be close to 90%, while the efficiency to find a correct fit, once the tracks were found was $\simeq$ 95%.

π^0-reconstruction

All showers in the gamma detectors with energy > 500 MeV and no charged tracks associated with them were used as gamma candidates. For showers in FGD one also required that the shower was initiated in the converter. The measured energy and the coordinates were used to compute the four-momenta of the gammas, assuming they originated in the centre of the bubble chamber. In order to reduce the combinatorial background from low energy gammas, cuts depending on the energy of the lower energy γ in the pair (see table 3) were applied on the χ^2-probability for the π^0 mass.

Table 3

π^0 probability cuts

$E_{\gamma_{min}}$	$P(M_{\pi^0})$
< 2 GeV	> 20%
2-4 GeV	> 10%
4-8 GeV	> 5%
> 8 GeV	> 1%

When applying these cuts, the signal to background ratio is 2:1. The combinations passing the cuts were used by the kinematical fit program which, for each decay hypothesis requiring a π^0, tried all candidates found.

Particle Identification

Particle identification was ensured through SAD and ISIS in complementary momentum ranges.

Knowing the momentum for a charged track passing through a SAD module, the theoretically expected numbers of photoelectrons for different masses are known. A χ^2-probability for the various mass assignments can be computed for the measured signal.

The sampling of the ionisation deposited by a particle traversing ISIS was made in up to 320 channels, with the regions of crossing tracks filtered out. This allowed us to compute the ionisation distribution. This Landau distribution depends on a scale parameter [12] which is proportional to the energy lost by the particle traversing the Ar/CO_2 mixture. A maximum likelihood fit to a model dE/dx distribution was performed giving the ionisation. The logarithm of the measured ionisation is normally distributed around the theoretical value, which can be computed when knowing the momentum of the particle. This enables us to compute a χ^2-probability for each mass assignment.

The information from the gamma detectors provided electron-hadron separation based on the comparison of the momentum measurement in the spectrometer and the energy released in the lead glass. In the FGD the efficiency is further improved by requiring that an electromagnetic shower is initiated in the first 5 radiation lengths, and that there is a good signal in the position measuring hodoscope. The resulting hadron rejection factor, for particles with momenta above 5 GeV/c, is of the order of 1:500 for FGD and 1:300 for IGD.

Kinematical Reconstruction

The final step in the data processing chain is the kinematic fitting which optimizes the track parameters $(1/P, \lambda, \phi)$ at a given vertex in order to satisfy energy and momentum conservation, subject to all mass assignments for the tracks that are compatible with the particle identification information. The kinematical fit program uses π^0 candidates found in the gamma detectors and neutral particles detected from their decay in the spectrometer. Each hypothesis was also tried with an unseen π^0 or K^0 included. Depending on the number of unmeasured quantities, the fit has 3, 2, 1, or 0 degrees of freedom (referred to as 3C, 2C, 1C or 0C fits in the following). A decay with only the momentum of the incident particle unmeasured will have 3 degrees of freedom, while a decay which in addition has an unseen neutral particle will have zero degrees of freedom. In this latter case no fit is performed, the program just propagates the errors to the unmeasured quantities.

3.5 Visibility, Acceptance and Geometrical Efficiency Corrections

The charm decays used in the following analysis were detected at scanning level. They must be given a visibility weight which compensates for losses at very short decay lengths, as well as for losses due to the finite size of the charm box and fiducial volume. This weight is a simple function of the minimum and maximum detectable decay lengths, l_{min} and l_{max}, respectively.

l_{min} is defined as the smaller of:

- The length necessary to observe a decay track not originating from the primary vertex at scanning with efficiency close to 1. This was taken as the distance along the line of flight necessary for at least one of the secondary decay tracks to achieve an impact parameter of 50 μm.
- The length necessary to detect the decay as an increase in ionisation. This length is the sum of two terms; the distance along the line of flight from the primary vertex to the point where the separation from the closest primary track is one bubble diameter, and the track length necessary to ensure that the increase is not a statistical fluctuation (e.g. for a C3 the track length that makes single and triple ionisation significantly different, assuming Poisson statistics).

l_{max} was computed taking into account the finite length of LEBC, the depth of focus and the boundaries of the charmbox.

A few decays ($\simeq$ 5% of the neutral sample) were found with a decay length smaller than the computed l_{min}: they were given a visibility weight $W_{vis} = 0$.

To take the geometrical acceptance of the spectrometer and the geometrical reconstruction efficiency into account, a spectrometer weight W_{SP} was computed for each decay with a kinematical interpretation. This weight was calculated by generating a large number ($\simeq 10^5$) of charmed particles with the same properties (x_F, p_t, decay channel) as the fit. For each generated decay, using our geometrical reconstruction and association efficiencies and our π^0 reconstruction efficiency we could determine for each simulated decay wether it leads to a fit with 3,2,1, or 0 degrees of freedom, or if it leads to an underconstrained solution (no fit). The spectrometer weight was defined as the ratio of the total number of generated decays to the number of decays belonging to the categories (normally fits with 3,2 or 0 degrees of freedom) accepted in the analysis of the real decays. For all the charm decay channels considered in the analysis the EHS spectrometer efficiencies (i.e. the inverse of W_{SP}) rise steeply around $x_F = 0$ to reach a nearly constant value, close to 1, above $x_F = 0$ for decays without neutrals and around $x_F = 0.2$ for decays with seen π^0. As an example we show in fig. 9 the efficiency to get kinematical fits for the decay $D^0 \to K^-\pi^+\pi^+\pi^-\pi^0$.

3.6 Background

We have studied three different sources of background to the charm sample; strange particle decays, secondary interactions with short (and undetected) recoil proton and background induced by incorrect associations between spectrometer tracks and bubble chamber tracks.

To estimate the background from the decay of strange particles, which affects the V2 and C3 topologies, strange particles (K, Λ and Σ) and their decays were generated according to known cross sections and branching ratios. These decays were then subjected to the cuts used in the analysis.

The remaining strange particle background in our fitted sample of charm decays in the V2 and C3 topologies is less than 0.10 events.

To evaluate the background from interacting particles we used a LUND Monte Carlo to generate the momentum spectrum for secondary particles. This was then used to generate secondary interactions, using the limitations imposed by the bubble chamber geometry, charm box etc. Interactions in which the recoil proton had a range less than 300 μm (this limit corresponding to more than 10 bubble diameters) were retained as potential background. Even with this rather conservative ansatz the background from this source, at scanning, is less than 0.2 events in both the charged and the neutral sample.

The possible background from incorrect associations between spectrometer tracks and bubble chamber tracks was estimated by generating K^0 and Λ^0 decays with complete events. All decays in the charmbox with one track in and one track out of the spectrometer acceptance were considered as background candidates. For these a false association was forced, using the closest track from the primary vertex. This new decay topology was then fed through the analysis chain. Using the upper limit probability of a false association the upper limit of this background in our fitted neutral charm sample was found to be less than 0.05 events.

4. RESULTS

4.1 Sample and Final Selection Criteria

The number of events in the charm box for different topologies is shown in the first row of table 4. For the C1 and V2 topologies the bulk of the events was removed as strange particles(*).

(*) Either by fits to strange decays or by the requirement of a decay $p_t > 250$ MeV/c.

For the C3 topology some events could be removed as ionisation jumps(*). After remeasurements 114 events remain, in which there are 183 candidates for charm decays, ie. 45 single charm candidates and 69 pairs. 100 of the charm decays are neutral and 55 are charged with $n_{charged} > 3$. In the analysis of D-mesons the C1 sample (28 decays) is not used, since it suffers from low kinematic fit efficiency and considerably lower scanning efficiency than the other topologies. All measured events were geometrically reconstructed and kinematically fitted. The number of decays for which we obtain kinematical fits with a charm hypothesis is given as "charm fits" in table 4. Some decays got several kinematical solutions. These ambiguities can occur between different charm particles or, for a given charm particle, between various decay modes and in some cases there are kinematical ambiguities for a well defined decay mode. Here we limit ourselves to a brief overview of the information available and how it has been used to resolve these ambiguities. Schematically the information used can be grouped into three categories; information on charged decay products from ISIS, knowledge of the spectrometer acceptance for neutral decay products and "a priori" knowledge about fit quality and the nature of charmed hadrons produced.

- The ISIS probability for the mass assignment e, π, K or p was considered, when larger than 4%, for each decay track. When this probability was larger than 20% for a given mass assignment, it turned out that it was less than 4% for any other mass. Consequently, only fits compatible with this unique mass assignment were selected. In all other cases, the fits compatible with the 4% cut in ISIS probability were accepted for further analysis.

(*) i.e. no track having an impact parameter larger than 7 μm.

When a kinematic solution was requesting the presence of unseen neutral particles, the number of unseen neutrals was checked against the quantity:

$$M^2 = m_i^2 + m_c^2 - 2m_i (m_c^2 + p_T^2)^{1/2}$$

where m_i is the mass of the incident charm particle, m_c the effective mass of the observed final state and p_T the transverse momentum of this system. A cut at $(M \pm \Delta M) = 400$ MeV was imposed to separate one π^0 from two π^0 solutions and at 700 MeV to separate K^0 from $(K^0+\pi^0)$ solutions.

Finally, if there was an ambiguity between several solutions using an unseen π^0, the solution with the π^0 which has the lowest detection probability was chosen.

- All other conditions equal, Cabibbo favoured fits were preferred over Cabibbo unfavoured, D-meson solutions over F-meson and Λ_c solutions and highly constrained fits over fits of lower constraint classes.

The results of this selection are given in Table 5 for the D^+ (D^-) and $D^0(\bar{D}^0)$ decays.

For the decays where there remained some ambiguities, but the x_F of all acceptable solutions differed by less than 0.1, one fit closest to the central value was chosen to represent the decay when using its physical quantities. The numbers given as "unique" in table 4 are the sum of this category of fits and of the genuinely unique fits in each topology. Table 5 gives some details on the final states which come out as the most probable ones according to this selection. It cannot be used, however, to extract information on branching ratios, etc., since these final states have not all the same detection efficiency.

The resulting distribution of the charged decays between the three charged charm particle states (D/F/Λ) is in perfect agreement with a maximum likelihood fit, not depending on these criteria. The maximum likelihood function was defined as a function of the transverse decay length and the χ^2 for the kinematical fit and the ionisation measurement, using the best fit (lowest χ^2) for each decay.

Table 4

Data Reduction for the Charm Sample

Number of prongs	1	2	3	4	5	6	7
In charm box at scanning	966	3399	192	21	7	1	1
Charm decays	28	78	51	22	4		
Charm fits	11	64	34	17	4		
"unique" fits	8	47	32	17	4		

Table 5

Charm final states giving a D-meson fit

$D^+ \to K^0\pi^+$	: 5(*)	$D^0 \to K^-\pi^+$	: 2
$K^0\pi^+\pi^0$	: 2	$K^0\pi^+\pi^-$	: 9
$K^-\pi^+\pi^+$	: 5	$K^-\pi^+\pi^0$	: 19
$K^0\pi^+\pi^+\pi^-$	: 11	$K^0\pi^+\pi^-\pi^0$	: 10
$K^0\pi^+\pi^0\pi^0$	: 1	$K^-\pi^+\pi^0\pi^0$	: 10
$K^-\pi^+\pi^+\pi^0$	: 6	$K^-\pi^+\pi^+\pi^-$	: 10
$K^0\pi^+\pi^+\pi^-\pi^0$	: 3	$K^-\pi^+\pi^+\pi^-\pi^0$	: 6
$K^-\pi^+\pi^+\pi^0\pi^0$	: 3	$\pi^+\pi^-$	: 1
$K^-\pi^+\pi^+\pi^+\pi^-$	: 2	$2\pi^+2\pi^-$	: 1
$3\pi^+2\pi^-\pi^0$	: 2	$K^+K^0\pi^-$	: 2
$\pi^+\eta K^0$	: 1	$K^+K^-\pi^0\pi^0$	: 1
Semileptonic:	5	Semileptonic:	10

(*) This channel being highly contaminated by the more frequent 3 and 4 body decays, we have kept in this table the 3C fit solution only.

4.2 Properties of the charmed D-mesons

The V2, C3, V4 and C5 topologies have been used for the analysis of the D-mesons. In the C3, V4 and C5 topologies the great majority of the decays is charm. This is not the case for the V2 topology, where the reduction from the total V2 sample (in the "charmbox") to the charm sample is by more than a factor 40. It has been shown that the remaining sample is free from strange particle background. It is however more difficult to prove that this reduction does not lead to biased losses of charm signal in the V2 topology. The most probable bias would be one against decays with very long lifetimes. When computing the lifetime from the V2 sample, with the same selection criteria as for the charged sample we arrive at $3.3^{+1.0}_{-0.7} * 10^{-13}$, in agreement with the lifetime derived from the V4 sample. This supports our conviction that the selection procedure for the V2 sample is free from biases. However since we use this consistency to verify that the V2-sample is unbiassed, the measurement of the lifetime from this sample is strictly speaking not an independent measurement. We therefore choose not to include this result in the determination of the lifetime.

D-meson Cross Sections

Since the EHS acceptance is small for $x_F < 0$, we quote as our main result cross sections for $x_F > 0$. We are however able to give an estimate for the total inclusive cross section for neutral D-mesons which agrees with our result for $x_F > 0$, assuming a roughly symmetric x_F distribution.

The cross section for neutral D-mesons has been evaluated by two different methods, one for the V4 sample and one for the V2 sample. The cross section analysis which uses the V4 data has been described in detail in a previous publication [2]. From 13 fitted decays the cross section was determined as:

$$\sigma(D^0/\bar{D}^0)=10.3 \pm 3.5 \ \mu b \text{ for } x_F > 0.$$

For the V2 sample a different approach has to be used, since the fraction of decays having a unique fit is considerably smaller than in the V4 sample due to the larger average number of neutrals in each decay. Therefore a method which does not rely on fit results was used. To determine the number of particles produced with $x_F > 0$ all charm candidate V2 with two hybridised tracks for which the longitudinal momentum, P_{long}, for the two tracks was larger than 16 GeV/c were used. A Monte Carlo calculation(*) was used to estimate how large a fraction of the decays with x_F larger than 0 have $P_{long} < 16$ GeV/c (7%)(**), and how large a fraction of the decays with $x_F < 0$ have $P_{long} > 16$ GeV/c (6%). To ensure that the topology is clear and has a high detection efficiency at scanning, visibility cuts were applied: The distance between primary and secondary vertices was required to be larger than 1.0 mm; the smaller impact parameter greater than 7 μm and the larger impact parameter greater than 50 μm. Corrections for these cuts were computed with a Monte Carlo technique, and the efficiency for associating tracks between the bubble chamber and the spectrometer was taken into account using the method described in section 3.5. The overall correction factor to the cross section from these cuts is 2.8 for events with $x_F > 0$.

(*) Unless explicitly stated otherwise all Monte Carlo calculations made to compute correction factors for D-mesons used the same assumptions: the D-mesons were generated according to $dN^2/dx_F dp_t^2 \; \alpha(1-|x_F|)^3 \exp(-1.1\, p_t^2)$. They were then assumed to decay according to phase space with mean lifetimes of $4.1*10^{-13}$s and $9.0*10^{-13}$s for neutral and charged mesons respectively. The decay channels used for the neutral decays and their assumed branching ratios were: $K^-\pi^+$ (2.6%), $K^-\pi^+\pi^0$ (9.3%), $K^-\pi^+\pi^0\pi^0$ (7.1%), $K^0\pi^-\pi^+$ (5.5%), $K^0\pi^+\pi^-\pi^0$ (4%), $e^+K^-\nu$ (8%). For the C3 topology, which is less sensitive to decay mode, the decays were assumed to be 1/3 into $K^-\pi^+\pi^+$, 1/3 into $K^-\pi^+\pi^+\pi^0$ and 1/3 into $\pi^+\pi^+\pi^-K^0$.

(**) This assumes that the x_F-distribution is symmetric around 0, which should be a reasonable assumption for the region close to 0, where the majority of the produced mesons ought to be found.

The uncertainties of the D^0 hadronic branching ratios and lifetime introduce a systematic error of 12% in this weight factor. There are five decays which are ambiguous between C3 and V2 topologies because the central track in a C3 decay has an impact parameter less than 7 μm, and the two remaining tracks have opposite charge. A Monte Carlo study has shown that only 5% of all genuine C3 decays will have this particular configuration, which makes the interpretation of them as V2 superimposed on a primary track plausible. We include these decays in the V2 sample and correct for the misinterpreted $D^{\pm}$. Finally, using our scanning efficiency for charmed V2 of 90 %, and the topological branching ratio $D^0 \rightarrow$ (two charged) of 67 ± 8% [18] we arrive at:

$$\sigma(D^0/\bar{D}^0) = 10.0 \pm 2.5 \text{ μb (based on 35.5 decays)}^{(*)}$$

Combining the results from the V2 and V4 topologies we get for the production cross section of neutral D-mesons at $x_F > 0$:

$$\sigma(D^0/\bar{D}^0) = 10.1 \pm 2.2 \text{ μb}.$$

This can be compared to the NA16 result: $\sigma(D^0/\bar{D}^0) = 7.7^{+7.2}_{-3.5}$ μb [19].

An attempt at estimating the total neutral D-meson cross section was made using all charm candidate V2 with $p_t > 250$ MeV/c, and all V4. For both topologies we only used events detected in the first two scan-passes. To compensate for losses at short distances all reconstructed strange decays were used. After correcting for the finite size of the bubble chamber and the effect of the scanbox cut, the strange particle length distribution is flat, except for the short decay length region, which is affected by low detection efficiency. Applying a correction for this to the neutral D-meson sample yields a total inclusive cross section:

$$\sigma(D^0/\bar{D}^0) = 24.3 \pm 5.5 \text{ μb (based on 76 decays)}.$$

(*) The visibility cuts do not leave the same number of events in the two views, hence the average value was used.

This method is not sensitive to a very backward $D^0/\bar{D}^0$ component, but assuming a symmetric x_F distribution this estimate is in good agreement with our determination of the cross section for $x_F > 0$.

The same method used to obtain the cross section for neutral D-mesons from the V2 sample was used to compute the cross section for charged D-mesons. All decays with three tracks fully reconstructed (32 decays) were used. To ensure that the final sample corresponds to production at $x_F > 0$ we require that the total visible longitudinal momentum of the decaying particle is larger than 20 GeV/c (the losses of decays with $x_F > 0$ and $P_{long} < 20$ GeV/c balance the influx of decays with $x_F < 0$ and $P_{long} > 20$ GeV/c). To ensure high scanning efficiency, and avoid topological ambiguities, we request that all three tracks have an impact parameter larger than 10 μm and at least one decay track has an impact parameter larger than 80 μm. (By chosing these cuts slightly more severely than in the V2 case, we achieve increased discrimination against Λ_c, in particular all previously identified Λ_c were rejected by this cut). The losses introduced by these selection criteria correspond to a correction factor averaged over the different decay modes of 2.65. The results presented here are stable against variations of the impact parameter cuts. In particular the result is stable when increasing the cut value for the larger impact parameter, which shows that there is no contamination from a short lived component. Including correction for the C3 charm scanning efficiency of 95 %, using the topological branching ratio ($D^{\pm} \geq 3$ charged) of 43 ± 5 % [18] and a sensitivity of 15.8 events per μb, we get,

$$\sigma(D^{\pm}) = 5.7 \pm 1.5 \text{ μb, for } x_F > 0 \text{ (based on 14 decays).}$$

The error can be divided into a statistical error and an estimated systematic error due to uncertainties in branching ratio and in life time of the order of 0.4 μb. This value can be compared to the NA16 result [19] of $\sigma(D^{\pm}) = 4.5^{+2.2}_{-1.4}$ μb.

X_F - and Transverse Momentum Distributions

For the determination of the x_F -distribution for D-mesons with $x_F > 0$ we used the decays selected according to the criteria given in section 4.1. In addition to these criteria we excluded decays requiring more than one neutral particle(*). Fitting the resulting sample of 57 events to $d\sigma/dx_F \alpha (1-x_F)^n$ we obtain $n = 3.8 \pm 0.6$ (fig. 10). If we separate the total sample of D-mesons into a "leading sample" which contains a valence quark which is also present in the incoming π^-(D^0, D^- and $\bar{D}^0$ from the seen decay of a D^{*-}) and a "non-leading sample" which does not ($\bar{D}^0$, D^+ and D^0 from the seen decay of a D^{*+}) a significant difference between the x_F -distributions is found. Performing the same fit as above we get $n = 1.8^{+0.6}_{-0.5}$ the "leading sample" (fig. 11a), and $n = 7.9^{+1.6}_{-1.4}$ (fig. 11b) for the "nonleading sample". A two component fit to the full sample with a fraction α of the D-mesons having $d\sigma/dx \simeq (1-x_F)^n$ and $(1-\alpha) \simeq (1-x_F)^m$ yields $\alpha = 0.80^{+0.10}_{-0.18}$ $n = 7.5^{+2.5}_{-1.7}$ and $m = 0.7^{+0.9}_{-0.7}$ (fig. 10). This agrees well with the NA16 [20] values of $\alpha = 0.7 \pm 0.3$, $n = 6 \pm 3$ and $m = 1 \pm 1$.

The same sample was used to determine the transverse momentum distribution of the D-mesons. Fitting $dN/dp_t^2 \simeq \exp(-bp_t^2)$ we obtain the best fit for $b = 1.0 \pm 0.1$ $(GeV/c)^{-2}$. (fig. 12). The average p_t^2 is 1.0 ± 0.1 $(GeV/c)^2$. The NA16 result for this fit was [21] $b = 1.1 \pm 0.3$ $(GeV/c)^{-2}$. The fitted values for the slope parameter for the "leading" and "nonleading" subsamples, as defined above, are in perfect agreement with each other.

(*) To obtain a constrained fit for this type of decays it is necessary to detect at least one neutral particle, thus introducing a possible background due to the low signal to background ratio for the π^0 detection. While studying production properties we can exclude these events, since their exclusion based on decay properties will not bias the production distributions.

We find no evidence for a correlation between x_F and transverse momentum of the charm particles. A more complete description of these distributions, and comparisons with production models is given elsewhere [22].

Fig. 13 shows the rapidity distribution of the full D meson sample used in this momentum distribution analysis.

D* production

In this experiment we detect a clear signal from charged as well as neutral D*. In fig. 14 we show the effective mass for 35 $D^0/\bar{D}^0\ \pi^{\pm}$ combinations, where for the 27 D-mesons with known charm quantum number only the "right sign" combination, i.e. $D^0\pi^+$ and $\bar{D}^0\pi^-$ are plotted. For D-mesons with undetermined charm quantum number pions of both charges were used to form the combinations. The shaded area represents a background estimation obtained by plotting "wrong sign" combination for the 27 D^0-mesons with known charm quantum number, and 22 combinations of charged D-mesons with charged pions. The computed D* cross sections indicate that the neutral D-meson production is fully saturated by D* production, while 48 ± 27% of the charged D-mesons originate from $D^{\pm}$*.

The D*-mesons are produced with a x_F -distribution: $d\sigma/dx_F \propto (1-x_F)^n$ with $n = 4.3^{+1.8}_{-1.5}$. No D* meson is produced with $x_F > 0.5$. The distribution of the transverse momenta for the D* mesons follows an exponential law: $d\sigma/dp_t^2 \propto \exp(-bp_t^2)$ with $b = 0.9^{+0.4}_{-0.3}$. A more detailed presentation of the production of D*-mesons is given in [23]

Mean Lifetimes

To determine the lifetime we used the unique kinematical fits. For these we performed a maximum likelihood fit, where the likelihood function was described by $L(\tau, l_{min}, l_{max}) = \Pi\tau^{-1} \exp(-t_i/\tau)/\{\exp(-t_{i\ min}/\tau)-\exp(-t_{i\ max}/\tau)\}$. The correction terms t_{min} and t_{max} are the decay times corresponding to the lengths l_{min} and l_{max} as described in 3.5. For the neutral D-mesons we have published [2] the values:

$\tau(D^0) = 3.5^{+1.4}_{-0.9} * 10^{-13}$ s based on eleven decays from the V4 sample.

Using the same technique for the charged sample, we obtain:

$\tau(D^{\pm}) = 9.8^{+3.4}_{-2.2} * 10^{-13}$ s (23 decays). These values are fully consistent with the NA16 values of $\tau(D^0)=4.1^{+1.3}_{-0.9} * 10^{-13}$ s from 16 decays and $\tau(D^{\pm}) = 8.4^{+3.5}_{-2.2} * 10^{-13}$ s from 15 decays respectively [21] and also with the present world averages [24] of $\tau(D^0) = 4.4^{+0.8}_{-0.6} * 10^{-13}$ s and $\tau(D^{\pm}) = 9.2^{+1.7}_{-1.2} * 10^{-13}$ s. The effects of the corrections for l_{min} and l_{max} are small. This can be seen from the fact that the average values for the proper time t, and $(t-t_{min})$ are 5.0 and 3.3 $*10^{-13}$s for the neutral decays, and 10.4 and 8.7 $* 10^{-13}$ s for the charged decays. Fig. 15 shows the $(t-t_{min})$ distributions of the D^0 and D^+ samples used for these life-time determination. The maximum likelihood values obtained have been tested for biases, both by varying the samples; using 3C/2C fits and 1C/0C fits separately; and by varying the parameters entering the computation of l_{min} and l_{max} (see 3.5). The results turned out to be stable to these variations and no systematic effects could be detected. As a further cross check we have estimated the lifetimes using a method which is independent of the kinematical fits. This method [25] makes use of the existing correlation between the average value of the impact parameters of the decay particles and the lifetime. The experimental values for the average of the impact parameters have been compared to the results from a Monte-Carlo analysis, taking the experimental efficiencies and the measured x_F and p_t-distributions into account. The results from that analysis were:

$\tau(D^0) = 6.5^{+1.9}_{-1.2} * 10^{-13}$ s for the V2 sample; sample(*)

$\tau(D^0) = 3.7^{+1.7}_{-0.8} * 10^{-13}$ s for the V4 sample;

$\tau(D^{\pm}) = 11.2^{+3.8}_{-2.6} * 10^{-13}$ s for the C3 sample.

(*) In the V2 sample there is a decay obtaining ambiguous fits with the proper time in the interval 17.2-35.4 $* 10^{-13}$ s. Having one event in the lower end of that range is perfectly consistent with a lifetime of $3.5 * 10^{-13}$ s, given the size of our sample. Removing this event from the impact parameter analysis gives the value $5.0^{+1.8}_{-1.1} * 10^{-13}$ s, whereas if it by chance would have had a unique fit with $t \simeq 20 * 10^{-13}$ s, the maximum likelihood fit value would, everything else unchanged, go up with about one sd.

The agreement between these two methods increases our confidence in the results from the likelihood fits, which we consider to be our best estimate of the mean lifetimes, since that method is model independent. Using the estimates from the maximum lieklihood fit we obtain for the ratio of the lifetimes for the charged and the neutral D-meson:

$$R = \tau_{D^\pm} / \tau_{D^0} = 2.8 \pm {}^{+1.3}_{-0.9}$$

Branching Ratios

To extract information on the number of decay products in our D-meson decay sample we used the distribution of maximum transverse momentum of the decay products. This distribution depends on the number of unseen neutral decay products, but not on the identity of the decay products. Hence the full sample of measured D decays could be used, without demanding kinematical fits. Performing a maximum likelihood fit of the Monte Carlo computed distributions, folded with our selection criteria gave the results shown in table 6 for $D^0/\bar{D}^0$ decaying into the V2 topology, and for $D^\pm$ decaying into the C3 topology.

Results on the branching ratios of D^+/D^- to 3 and 5 prongs and of $D^0/\bar{D}^0$ to 2 and 4 prongs are given in table 7 and discussed in detail elsewhere [27]. In the same reference a detailed analysis of the charged kaon and electron content of the charm decay tracks is described. The results are also given in table 7. The cleanliness of the electron signal is apparent from the ionisation data shown in fig. 16. The systematic errors on the results are negligible. We note that the D^0 semi-electronic branching ratio is greater than 0.11 at the 90% confidence level [27] which is incompatible with published results from Mark III [26].

Table 6

D meson decay multiplicities

$D^0/\bar{D}^0 \rightarrow$ V2 topology

2-body	$5 \pm 3\%$
3-body	35^{+21}_{-16}
4-body	60^{+21}_{-30}
5-body	<20 %
6-body	<2 %

$D^{\pm} \rightarrow$ C3 topology

3-body	$16 \pm 6\%$
4-body	$65 \pm 16\%$
5-body	$19 \pm 10\%$
6-body	< 2%

Table 7

Branching ratio summary

$D^{\pm}$	$D^0/\bar{D}^0$
$\frac{\text{all C5}}{\text{all C3}} = 0.09 \pm 0.05$	$\frac{\text{all V4}}{\text{all V2}} = 0.25 \pm 0.07$
In C3: Ratio of decays with $K^{\mp} = 0.32^{+0.15}_{-0.13}$	In V2: Ratio of decays with $K^{\pm} = 0.51 \pm 0.14$ In V4: Ratio of decays with $K^{\pm} = 0.52^{+0.31}_{-0.23}$
$\frac{D^{\pm} \rightarrow e^{\pm} + \text{Charged hadrons}}{\text{All } D^{\pm} \rightarrow \text{C3}} = 0.07^{+0.08}_{-0.05}$	$\frac{D^0/\bar{D}^0 \rightarrow e^{\pm} \text{ inclusive}}{\text{all } D^0/\bar{D}^0} = 0.15^{+0.08}_{-0.06}$

4.3 Search for the charmed $F^{\pm}$ meson

In our sample of charged decays we have no unambiguous F decay. We have used the C3 sample to search for $F^{\pm} \rightarrow K^{\pm} + X$, (where X is 2 charged + n neutrals) [28]. In this search we defined a $K^{\pm}$ as a track for which kaon is the best mass assignment in ISIS, and for which the second best mass assignement has a probability less than half of that of the K-hypothesis. With these criteria we find no decay with a kaon with the same sign as the parent particle. In order to convert this result into a cross section we used a Monte Carlo technique to evaluate the detection

Table 8

$\sigma \cdot B$ for $F^{\pm} \rightarrow K^{\pm}X$ and $\Lambda_c^{\pm} \rightarrow p^{\pm}X$ as a function of $\tau(F)$ and $\tau(\Lambda_c)$

$\tau \cdot 10^{-13}$ s	0.5	1.0	2.0	3.0	4.0
$\sigma \cdot B(F)(\mu b)$	< 5.0	< 1.4	< 0.8	< 0.6	< 0.5 (90% CL)
$\sigma \cdot B\ (\Lambda_c)(\mu b)$	$3.2^{+4}_{-2}{}^{.2}_{.1}$	$1.0^{+1}_{-0}{}^{.3}_{.7}$	$0.5^{+0}_{-0}{}^{.7}_{.4}$	$0.4^{+0}_{-0}{}^{.5}_{.3}$	

efficiency for these selection criteria. F-mesons were generated according to $d^2N/(dx_F dp_t^2) = (1-x_F)^n \exp(-1.1p_t^2)$, with different assumptions for n and the F lifetime. The ionisation in ISIS was simulated to determine the particle-identification probabilities, and from this we determined the fraction of decays which would have been detected. In this way we obtained the 90% confidence level upper limits shown in Table 8 for the inclusive F cross-section σ, times B, the branching ratio $F^{\pm} \rightarrow K^{\pm} + X$, for different F lifetimes and for n = 3.

efficiency for these selection criteria. F-mesons were generated according to $d^2N/(dx_F dp_t^2) = (1-x_F)^n \exp(-1.1 p_t^2)$, with different assumptions for n and the F lifetime. The ionisation in ISIS was simulated to determine the particle-identification probabilities, and from this we determined the fraction of decays which would have been detected. In this way we obtained the 90% confidence level upper limits shown in Table 8 for the inclusive F cross-section σ, times B, the branching ratio $F^{\pm} \to K^{\pm} + X$, for different F lifetimes and for n = 3.

4.4 Search for the charmed Λ_c baryon:

In the C3 sample we have three Λ_c (3 constraints fits) for decays fulfilling the cuts described in section 4.1. These three 3C fits are summarised in Table 9.

Table 9

Main Characteristics of the three unique Λ_c

Id	Decay Mode	Mass	x_F	P_t	t	t_{min}
		(GeV/c^2)		(GeV/c)	10^{-13}s	10^{-13}s
1	$\bar{\Lambda}^0\ \pi^+\pi^-\pi^-$	2.291	0.24	0.911	1.25	1.12
2	$K^+\pi^-\bar{p}$	2.275	0.09	0.901	1.92	2.95
3	$K^-p\pi^+$	2.283	0.33	1.304	2.87	2.12

The characteristics of these events are;

event 1: The decay of the $\bar{\Lambda}$ into $\bar{p}\pi^+$ is observed in the bubble chamber, and has a unique kinematical fit with the C3 vertex as production point. For the antiproton from this decay no particle identification is available. All other decay products are uniquely identified as pions. There is no charm partner found in this event.

event 2: From this decay the antiproton and the π^- are uniquely identified, while the positive track has no identification information. In this event there is also a C3 which fits a $D^+ = > K^-\pi^+\pi^+$, with the K^- and one of the pions identified.

event 3: In this decay the proton is uniquely identified, while the other two decay products are π/K ambiguous. The accompanying decay in this event is a $\bar{D}^0 \rightarrow K^+\pi^-\pi^0$, with the π^- out of the spectrometer acceptance, and hence unidentified, and the π^0 reconstructed from the gamma detectors.

The average value for the mass of the three decays in Table 8, 2.283 agrees well with the world average [24]. As for production properties one might note the high value for average p_t, 1.04 GeV/c, and that the two events with positive x_F both have rather high x_F-values. But ambiguous events which have been called D-mesons due to the selection rules might populate the low x_F region preferentially(*). As long as we suffer from low statistics this effect cannot be corrected for, and might explain part or all of this behaviour. The average value of $(t-t_{min})$ for the two events with $t > t_{min}$ is $0.44 * 10^{13}$ s. It has been verified that this sample is free from strange particle background by the same method as described in 3.5, and also by checking the effective mass of all pairs of opposite charge. Another possible source for background is misinterpreted D-mesons. To investigate this we generated $D^{\pm}$ into $K\pi\pi$, $K\pi\pi\pi^0$ and $K\pi\pi\pi^0\pi^0$. Applying our cuts to the generated decays and demanding a kinematical fit as a unique Λ_c together with particle identification constraints we estimate the background for these three decays from misinterpreted D-mesons to be $\simeq 0.04$ events.

(*) This is in fact supported by a Monte Carlo study of the decay into $pK\pi\pi^0$ and $\Lambda^0\pi\pi\pi$, for which at low x_F values the probability to obtain a 0C solution (which would be overridden by the selection rules) is higher than to obtain a 3C fit.

An order of magnitude estimate of the cross section for $x_F > 0$ can be obtained using event 3, for which the branching ratio is known [24] to be 2.2%. Using the visibility weight and acceptance correction, as described in section 3.5, but no corrections for losses due to ambiguities at short distances, we arrive at an inclusive cross section of ≈ 4.5 μb for $x_F > 0$. To compute a cross section times branching ratio for ($\Lambda_c \rightarrow$ p + 2 charged + X) an approach similar to the one for F-mesons was used. To ensure high visibility and a measurement of good quality, and avoid severe topological ambiguities all C3 decays were subjected to the following cuts;

- a decay length > 500 μm;
- at least one track having an impact parameter larger than or equal to 25 μm at the secondary vertex;
- no more than one track with impact parameter < 7 μm at the primary vertex.

Since the Λ_c is expected to have a lifetime of the order of $1\text{-}2 * 10^{-13}$ s one might expect the majority of the decays to be close to the primary vertex, where topological ambiguities might be important. In order to take this into consideration also V2 decays having the secondary vertex obscured were considered if they had;

- a decay length larger than 500 μm;
- the larger impact parameter > 25μm and the smaller > 7 μm;
- at least one primary track closer than 7 μm to the secondary vertex.

These selection criteria leaves 50 decays from the C3 topology and 16 from the V2 topology. Together these decays have 110 tracks for which there exists particle identification from ISIS. For five of these the probability for the proton hypothesis is more than two times higher than for any other hypothesis, and these five decays (all from the C3 topology) are then considered as having an identified proton. Two of these events have a seen charged momentum larger than 26 GeV/c and thus definitely have $x_F > 0$. They form our sample for the calculation of the cross section times branching ratio for $x_F > 0$. To correct for the cuts applied

Λ_c were Monte Carlo generated(*) with varying assumptions about the lifetime. For each decay track the ionisation in ISIS was generated, with its corresponding error. Applying the cuts described above to the generated events it is possible to compute a correction factor. This factor varies within less than 10% when varying the exponent for the x_F dependence between 1 and 7, and $\simeq$ 10% when making different assumptions about the branching ratios for Λ_c. Since this is small compared to our statistical errors we compute the cross section times branching ratio using the factor obtained with the exponent = 3, and for the $pK^-\pi^+\pi^0$ channel. Using the experimental sensitivity of 15.8 events/μb and the C3 scanning efficiency of 95% we obtained the values shown in table 8. Assuming a life-time of 10^{-13} s and an inclusive branching ratio $\Lambda_c \to p+x$ of 25%, we estimate $\sigma(\Lambda_c) \sim 4^{+5}_{-3}$ μb for $x_F > 0$.

4.5 Correlation Between Charmed Particles

This experiment provides the opportunity to study correlation properties of $D\bar{D}$. The general strategy for selecting events in this study is the same as described in 4.1. This procedure leads to a sample of 12 $D\bar{D}$ pairs in which the x_F of the pair has $x_F > 0$, and each individual D has $x_F > -0.1$. The total weight for these events is 35.6. The rapidity gap distribution for these events is shown in fig. 17a. In the plane transverse to the beam direction an important physical quantity is the angle between the two charm particles, ϕ_T. Since this quantity can be computed merely from a knowledge of the decay vertices we use a larger sample of pairs rejecting only those events in which the error on $\cos\phi_T$ is greater than 0.2. The ϕ_T distribution corresponding to 30 such pairs is shown in fig. 17b.

The curves superimposed on the experimental distributions of figs. 17a and 17b have been obtained with a simple model which assumes uncorrelated DD pair production (except for momentum conservation). They give a reasonably good first approximation to the data. A more detailed discussion of these results is given in [29].

(*) The decays were generated according to $d^2\sigma/(dx_F dp_t^2) \alpha (1-x_F)^n \exp(-1.1\ p_t^2)$ $(x_F > 0)$ in five different decay channels; $pK^-\pi^+$, $pK^-\pi^+\pi^0$, $p\pi^-\pi^+K^0$, $pK^-\pi^+\pi^0\pi^0$ and $p\pi^-\pi^+K^0\pi^0$.

5. DISCUSSION OF THE RESULTS

We have measured the total charm hadron cross section at positive x_F in 360 GeV/c π^- proton interactions to be 20.2 ± 4.8 μb. (15.8 ± 2.7 μb for charmed D mesons). The cross section is dominated by D-meson production, being 10.1 ± 2.2 μb for $D^0/\bar{D}^0$ and 5.7 ± 1.5 μb for D±. It includes a contribution of ≃ 4.5 μb for Λ_c production. D* production accounts for nearly all the neutral D-mesons produced and for 55 ± 30% of the charged D-mesons.

To evaluate these cross sections we have used topological branching ratios. These are much more precisely determined than the exclusive branching ratios and do therefore contribute very little to the systematic uncertainty. Our cross section determination needs no correction for the atomic number dependence of the target since pure hydrogen is used. The minimum bias interaction trigger had a very high efficiency (98%) for charm events. Systematic effects due to the spectrometer acceptance are negligible at $x_F > 0$, and the effect of visibility corrections is relatively small. The average visibility weight at $x_F > 0$ is 1.76. The only other experiments which have measured charm hadron cross-section in π^- proton interactions are NA16, also using a 360 GeV/c π^- beam, with which the NA27 results are in good agreement ($\sigma_{tot}(x_F > 0) = 12.2^{+8}_{-4}$ μb) [19] and an experiment done at BNL with the Magnetic Spectrometer [30] which found an upper limit of 150 nb at 95% C.L. using 16 and 17 GeV/c π^- beams. Another experiment using a similar technique to NA27 has measured the charm pair cross section in 360 GeV/c π^- nucleon interactions [31]. The charm decays were observed in a heavy liquid bubble chamber and yielded a total $D\bar{D}$ production cross-section of (28 ± 11) μb/nucleon assuming an A^α dependence with $\alpha = 1$, and (72 ± 27) μb/nucleon assuming $\alpha = 2/3$. This cross section is approximatively equal to the inclusive cross section for $x_F > 0$ if most of the charm production is central. Another experiment, detecting the prompt single muon produced in 278 GeV/c π^--Fe interactions [32], and assuming a linear A dependence and an average muon branching ratio of 8%, found a cross section for inclusive $D\bar{D}$ production at $x_F > 0$ of $17.5^{+5.4}_{-3.9}$ μb/nucleon (with $\alpha = 2/3$, the cross-section would be 67 μb/nucleon). The good agreement between these experiments and NA27 speaks in favour of a global linear dependence of the cross section on the atomic number of the target. The accuracy in these experiments is not good enough to determine how this A dependence varies with

the longitudinal momentum of the charm hadrons. The results obtained by [33] with incident π^- at 120, 175 and 200 GeV/c on beryllium are not sufficiently accurate to be used in this comparison (they find $\sigma(D\bar{D}+X) = 48 \pm 15 \pm 24$ μb/nucleon at 175-200 GeV/c and σ(120 GeV/c)/ / σ(175-200 GeV/c) = 0.62 ± 0.34, assuming an A^1 dependence). The p_t distribution of the charm hadrons follows the standard exponential law $\alpha \exp(-bp_t^2)$ with b=1.0 ± 0.1 $(GeV/c)^{-2}$. This value is in good agreement with the values observed by NA16 (1.1 ± 0.3) and [34], (1.1 ± 0.5), and is larger but still compatible with [32] (0.70 ± 0.15).

We definitely observe a leading particle effect when we separate our sample into "leading D" and "non-leading D" again in agreement with the first evidence observed in NA16 [21], and with the large asymmetry between the μ^+ and μ^- production observed by [32] but in sharp contrast with the conclusion drawn by [34]. A two component fit to the full sample gives a good representation of our data, with a dominant "central" production (n = 7.5) and a less important but significant flatter distribution (n = 0.7). The D*-mesons are centrally produced with $d\sigma/dx_F \alpha (1-x_F)^n$ where the best fit value for n is 4.3. No D* with $x_F > 0.5$ is observed.

A comparison of these production properties with the QCD fusion models can be found in [22]. Insight on these production schemes may also come from the information collected on the correlations between the two charm hadron particles since for most of our data we observe the $D\bar{D}$ pair. The expected short range correlation is not confirmed by the observed rapidity gap distribution. However, a clear correlation is observed on the transversal angular distribution of the two charm hadrons; part of it is of course a simple consequence of transversal momentum conservation (which would lead to a strict colinear behavior if the pions associated to the $D\bar{D}$ pair in a given event average to $\Sigma p_t = 0$), but the dynamics of the charm production must also account for the observed distribution. A more detailed analysis of these correlation effects can be found in [29].

6. ACKNOWLEDGEMENTS

We are indebted to the CERN staff, whose sterling performance was essential in collecting the data for this experiment. We also would like to take the opportunity to acknowledge the heroic effort by our scan and measurement personel in the participating labs.

REFERENCES

[1] M.E. Michalon-Mentzer, 19th Rencontre de Moriond, March 1984 Vol. 2, p. 267, Editions Frontieres (edited by J. Tran Thanh Van).
J. Hrubec, 22nd International Conference on High Energy Physics, July 1984 (Leipzig), Vol.1, p.159, (edited by A. Meyer and E. Wieczorek).

[2] M. Aguilar-Benitez et al., Phys. Lett. 146B (1984) 266.

[3] M. Aguilar-Benitez et al., Nucl. Instrum. Methods, 205 (1983) 79.

[4] P. Coet, N. Doble and S. Reucroft, Beam possibilities for EHS CERN/SPS 81-25 (1981) and contained in Yellow Report CERN 82-10 (1982).

[5] H. van Brungel and N. Siegel, A pulsed magnet system to modulate the beam for rapid cycling bubble chambers, CERN/SPS 81-13 (1981).

[6] J.L. Benichou et al., Nucl. Instrum. Methods (1981) 487.

[7] F. Bruyant et al., Nucl. Instrum. Methods 176 (1980) 409.

[8] R.J. Gray, Nucl. Instrum. Methods 176 (1980) 133.

[9] T. Modis, Nucl. Instrum. Methods 176 (1980) 129.

[10] A. Bettini et al. Nucl. Instrum. Methods 204 (1982) 65.

[11] P.J. Carlson et al. Nucl. Instrum. Methods 192 (1982) 209.

[12] W.W. Allison and J.H. Cobb, Annual Review of Nuclear Particle Science (39) (1980) 253.

[13] W.W.M. Allison and P.R.S. Wright, Formulae and Methods in Experimental Data Evaluation, Vol.2, eds. R.K. Bock et al. European Physical Society, Jan. 1984

[14] W.W.M. Allison et al., Nucl. Instrum. Methods 224 (1984) 396.

[15] B. Powell et al., Nucl. Instrum. Methods 198 (1982) 217.

REFERENCES (cont'd)

[16] A. Firestone et al., Phys. Rev. D14 (1976) 2902.

[17] J.R. Lutz, A. Michalon, II Vezelay Workshop on EHS, CERN/EP-EHS/PH 80-2.

[18] G.H. Trilling, Phys. Rep. 75 (1981) 57;
I. Peruzzi et al., Phys. Rev. Lett. 39 (1977) 1301;
R. Schindler et al., Phys. Rev. D24 (1984) 78.

[19] M. Aguilar-Benitez et al., Phys. Lett. 135B (1984) 237.

[20] M. Aguilar-Benitez et al., Phys. Lett. 123B (1983) 98.

[21] M. Aguilar-Benitez et al., Phys. Lett. 122B (1983) 312.

[22] M. Aguilar-Benitez et al., Inclusive properties of D-mesons- (submitted to Phys. Lett.)

[23] M. Aguilar-Benitez et al., Neutral and charged D* production in 360 GeV/c π^- p interactions (to be submitted to Phys. Lett.)

[24] Particle Data Group: Review of Particle Properties,
Reviews of Modern Physics, Vol.56, No.2, Part 2, April 1984.

[25] S. Petrera and G. Romano, Nucl. Instrum. Methods 174 (1980) 61;
P. Checchia et al., Internal INFN/PD/EHS 84 (1984).

[26] R.M. Baltrusaitis et al., Phys. Rev. Lett. 54 (1985) 1976.

[27] M. Aguilar-Benitez et al., Direct measurement of the charmed D^+ and D^0 branching ratios (to be submitted to Phys. Lett.).

[28] M. Aguilar-Benitez et al., A search for F production in 360 GeV/c π^- p interactions (to be published in Phys. Lett.).

[29] M. Aguilar-Benitez et al., $D\bar{D}$ correlations in 360 GeV/c π^-p interactions (to be submitted to Phys. Lett.).

REFERENCES (cont'd)

[30] S.U. Chung, Proceedings of the Moriond Workshop on New Flavours 1982 (Editions Frontieres).

[31] A. Badertscher et al., Phys. Lett. 123B (1983) 471.

[32] J.L. Ritchie et al., Phys. Lett. 138B (1984) 213.

[33] R. Bailey et al., Phys. Lett., 132B (1983) 230.

[34] R.Bailey et al., Phys. Lett. 132B (1983) 237.

FIGURE CAPTIONS

Fig. 1 The version of the European Hybrid Spectrometer used for the NA27 π^- exposure.

Fig. 2 The chamber body of LEBC II, fabricated from LEXAN. Within the upper part of the rectangular frame the shrinked metallic circular seals for valve, gauge and heat-exchanger are visible.

Fig. 3 Vertical cut through the optics plane.

Fig. 4 A typical quality photograph of an untypically clear decay. In this event there is one C3 and one C1 decaying in the bubble chamber (cf. fig. 8).

Fig. 5 The charged multiplicity distribution at primary vertex, compared to Firestone et al. [16] (note that the statistical errors of this experiment are smaller than in [16]).

Fig. 6a Definition of the concept of impact parameter; $y = L\sin\varphi$.

Fig. 6b Definition of the "scan box". Each event was scanned for secondary activity inside the dashed line, a rectangle of width ±2 mm centered on the interacting beam. Also shown is the definition of L and θ, as used in section 3.3.

Fig. 7 Distribution of the parameter $|L \sin\theta|$ for the charm sample. L and θ as defined in figure 6b.

Fig. 8 An HPD digitization of the same event as in figure 4. The primary vertex is located at point A, a C3 decay at point B and a C1 decay at point C.

Fig. 9 The efficiency for EHS to obtain a 3C, 2C or a 0C fit for the decay $D^0 \to K^-\pi^+\pi^+\pi^-\pi^0$, as a function of x_F ($\epsilon = 1/W_{sp}$).

Fig. 10 The x_F-distribution for the D-meson sample (57 decays). Superimposed is the fit result: dN/dx_F prop. to $(1-x_F)^{3.8}$ (fig. 10a); and the result of a two component fit: $0.80\ (1-x_F)^{7.5} + 0.20\ (1-x_F)^{0.7}$ (fig. 10b).

Fig. 11a The x_F-distribution for the D-mesons containing a "leading quark", as defined in the text. The curve superimposed is the fit result: dN/dx_F. prop. to $(1-x_f)^{1.8}$.

FIGURE CAPTIONS (cont'd)

Fig. 11b The x_F-distribution for the D-mesons not containing a "leading quark", as defined in the text. The curve superimposed is the fit result: dN/dx_F. prop. to $(1-x_F)^{7.9}$.

Fig. 12 The p_t^2 distribution for the full D-meson sample.

Fig. 13 The rapidity distribution of the full D-meson sample.

Fig. 14 The $D^0/\bar{D}^0$ $\pi^{\pm}$ effective mass spectrum. For D mesons with known charm quantum number $D^0\pi^+$ or $\bar{D}^0\pi^-$ combinations are plotted, for ambiguous decays all combinations are plotted. The shaded area is the background estimation as explained in the text.

Fig. 15 $(t-t_{min})$ distributions of the $D^0/\bar{D}^0$ and $D^{\pm}$ samples used for the lifetime determination.

Fig. 16 Ionisation versus momentum as measured in ISIS for 7 semi-electronic decays (C3 and V2). Dots are for identified electrons, squares for π, triangles for K and the cross-point is a π/k ambiguous track.

Fig. 17a Difference in rapidity between D and $\bar{D}$ in 12 fully reconstructed $D\bar{D}$ pairs.

Fig. 17b The angle in the transverse plane, φ_T between D and $\bar{D}$ in 30 geometrically reconstructed pairs.

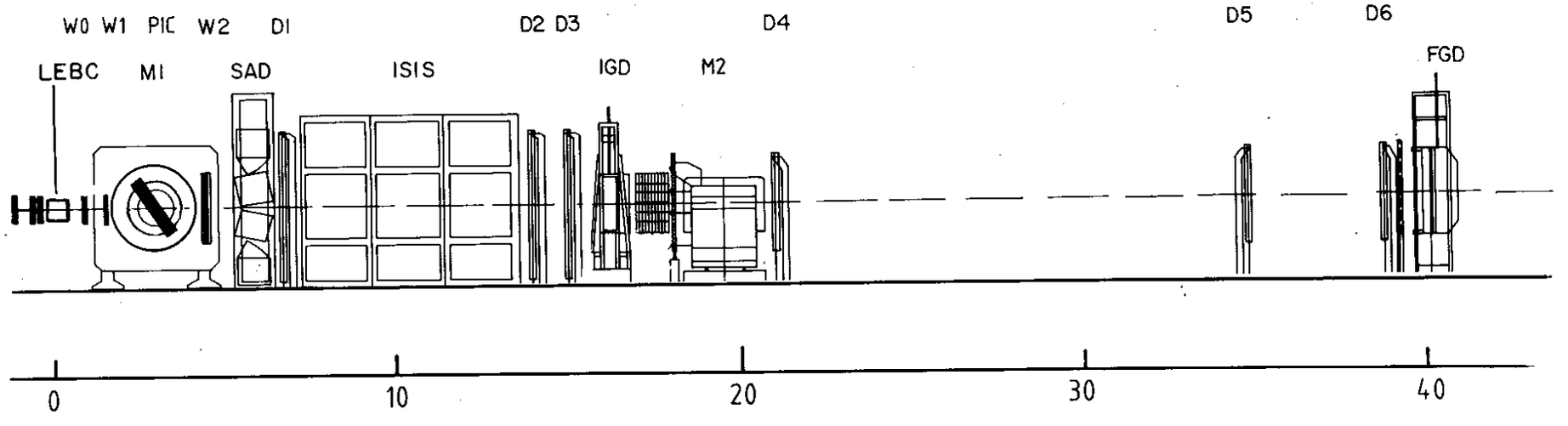
W0 W1 PIC W2 D1
D2 D3
D4
D5
D6
LEBC
M1
SAD
ISIS
IGD
M2
FGD
0
10
20
30
40

FIG. 1

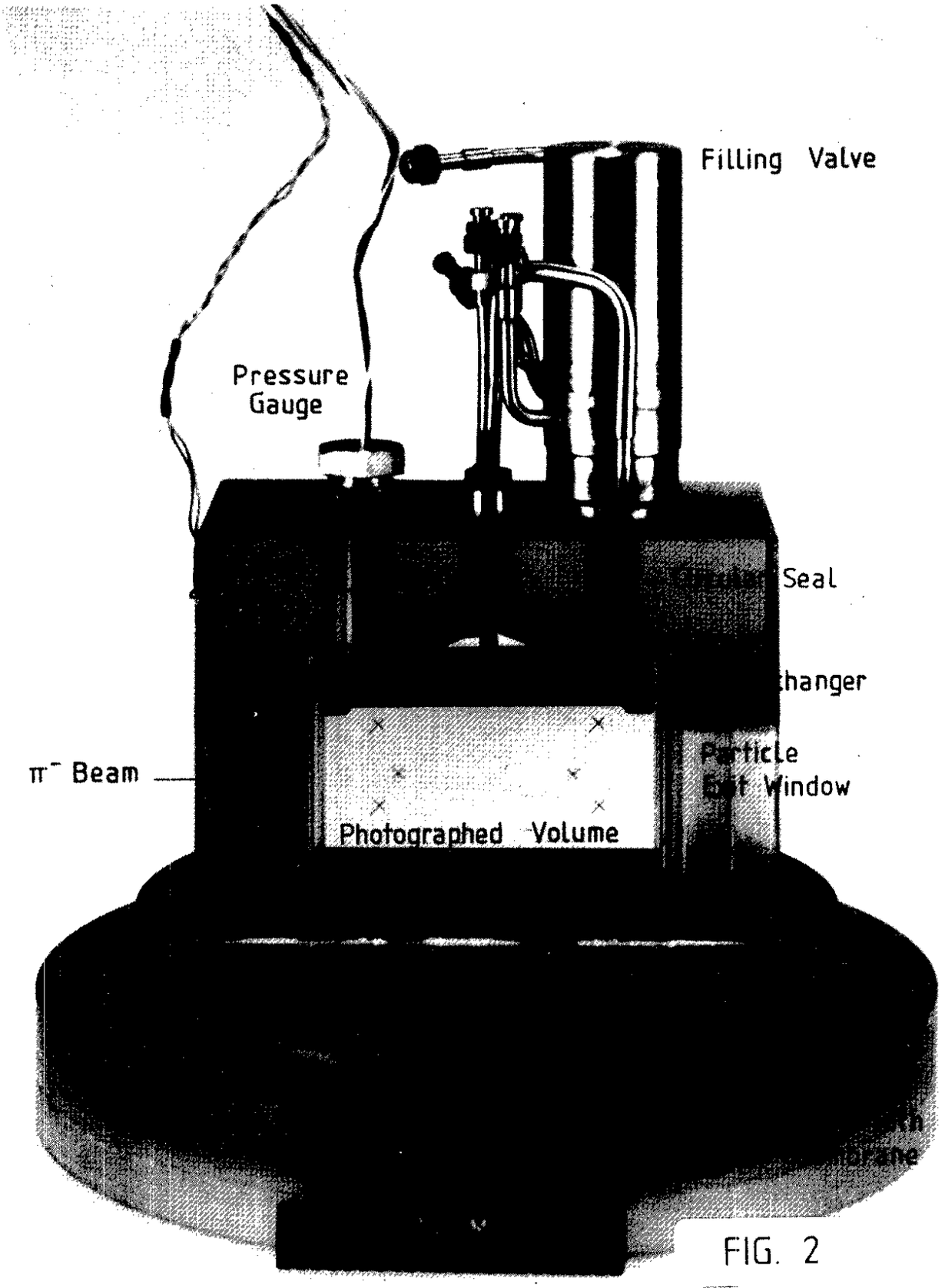
Filling Valve
Pressure Gauge
Seal
hanger
Particle
Window
π⁻ Beam
Photographed Volume

FIG. 2

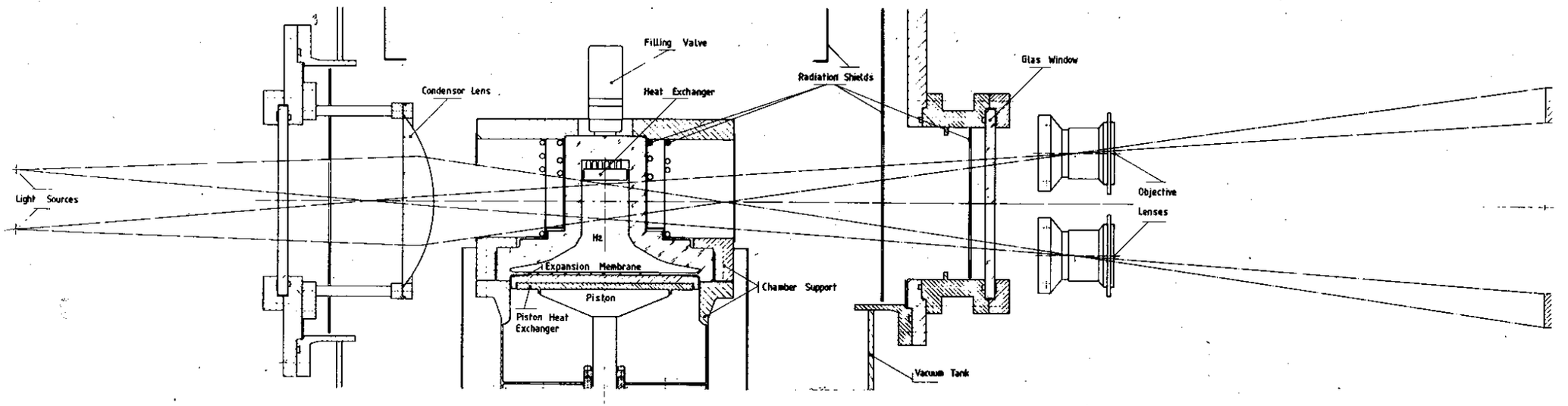
Filling Valve
Condensor Lens
Heat Exchanger
Radiation Shields
Glas Window
Light Sources
Objective
Lenses
Hz
Expansion Membrane
Chamber Support
Piston
Piston Heat
Exchanger
Vacuum Tank

FIG. 3

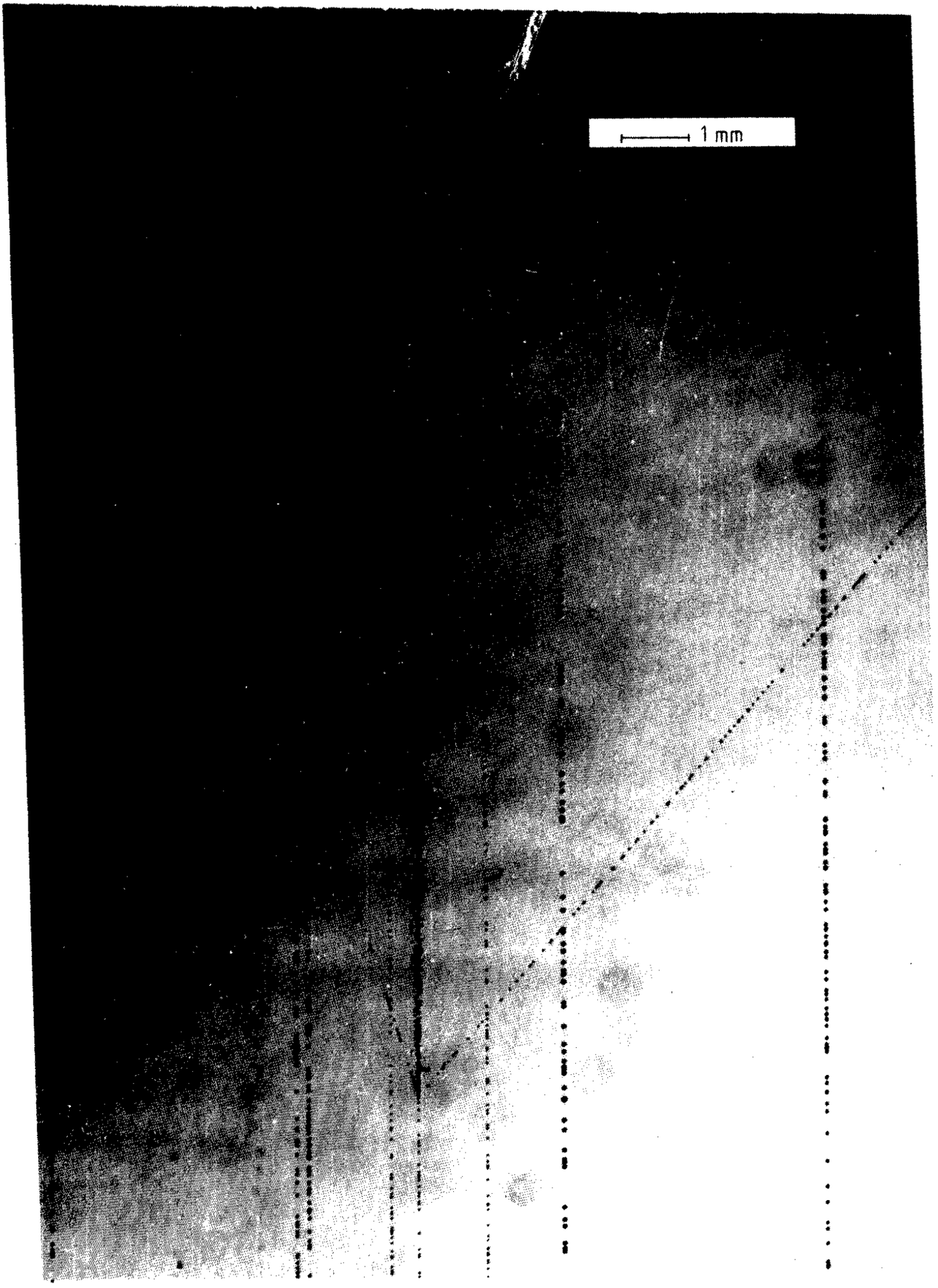

FIG. 4

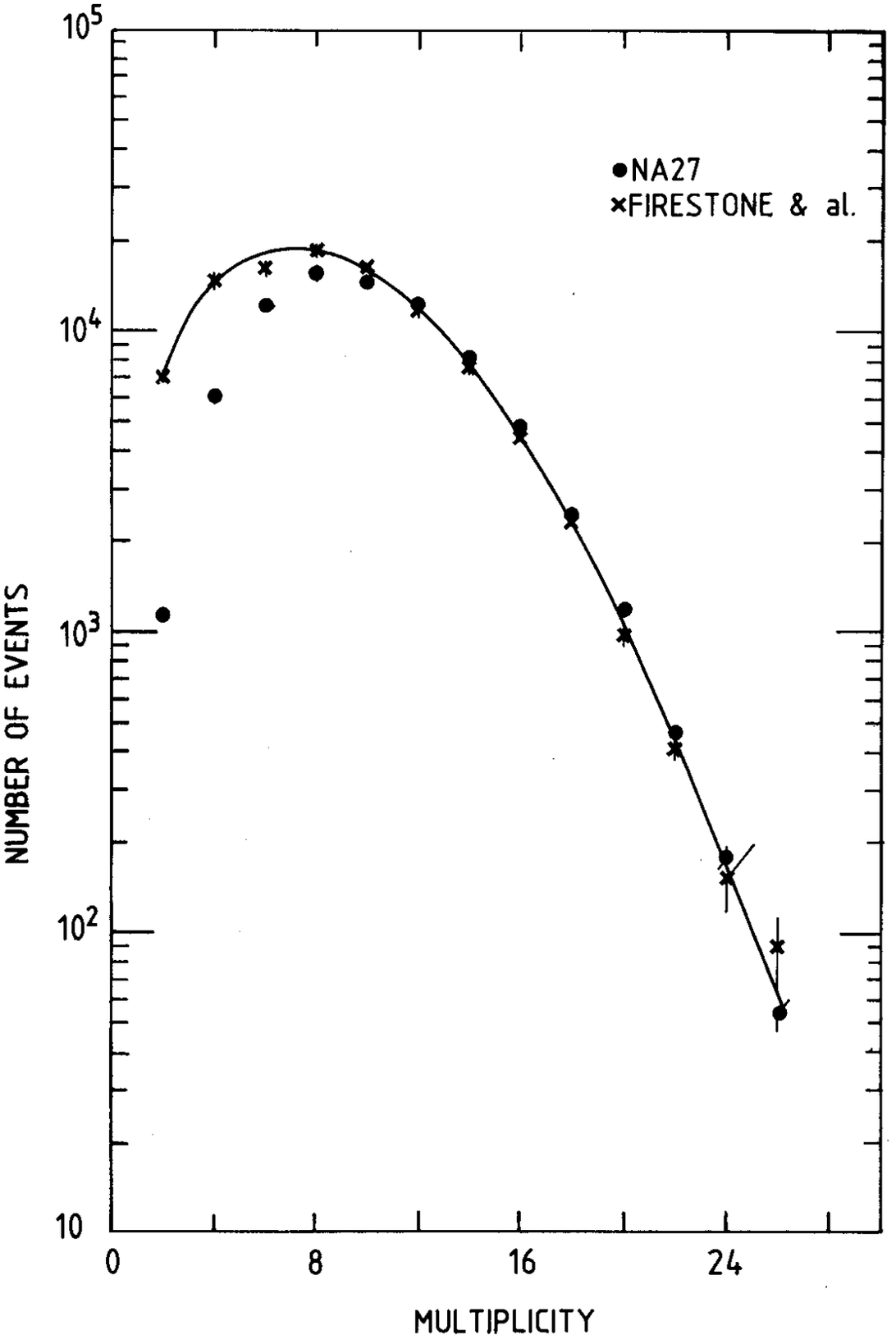
10^5
10^4
10^3
10^2
10
NUMBER OF EVENTS
●NA27
×FIRESTONE & al.
0
8
16
24
MULTIPLICITY

FIG. 5

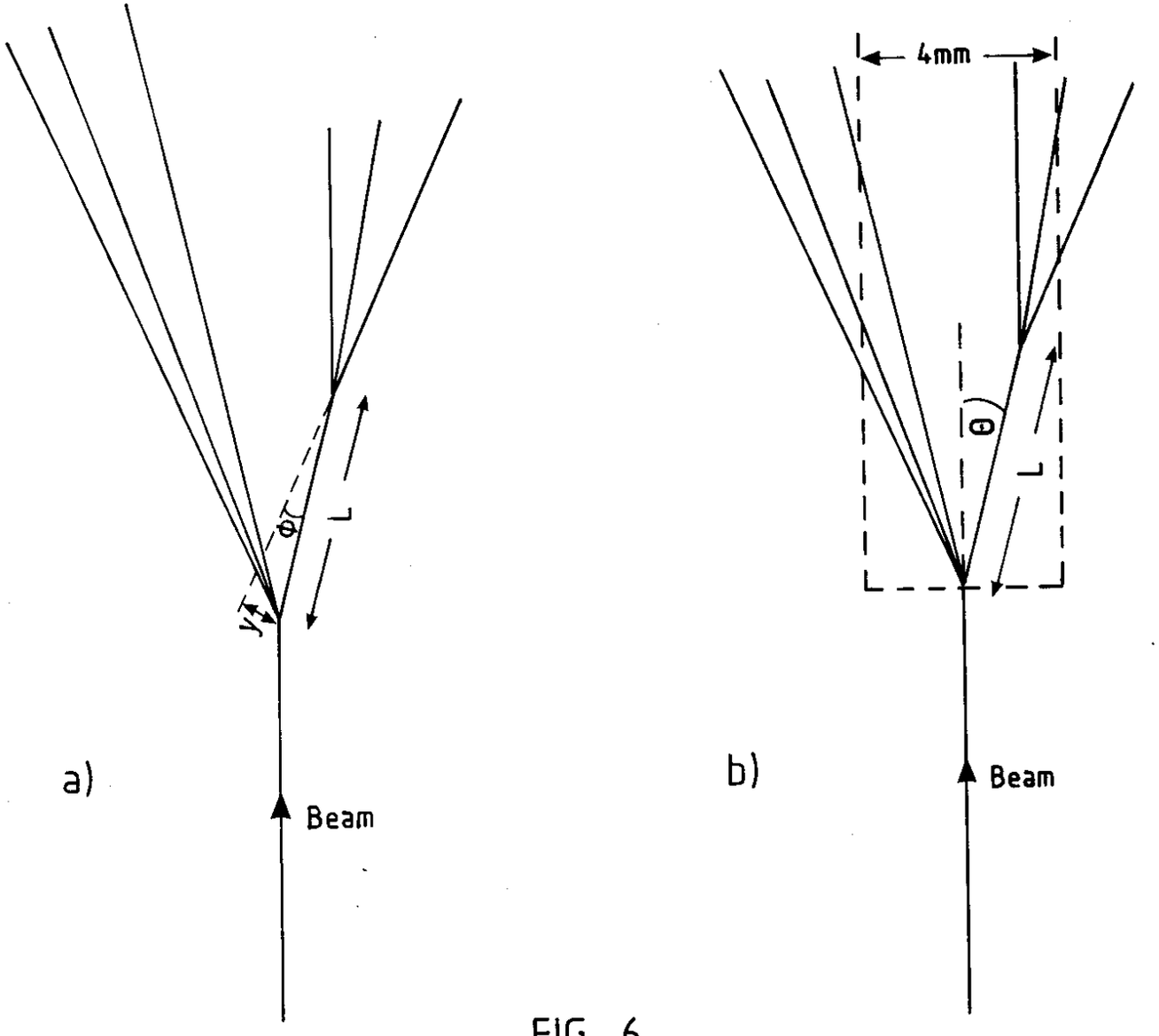

FIG. 6

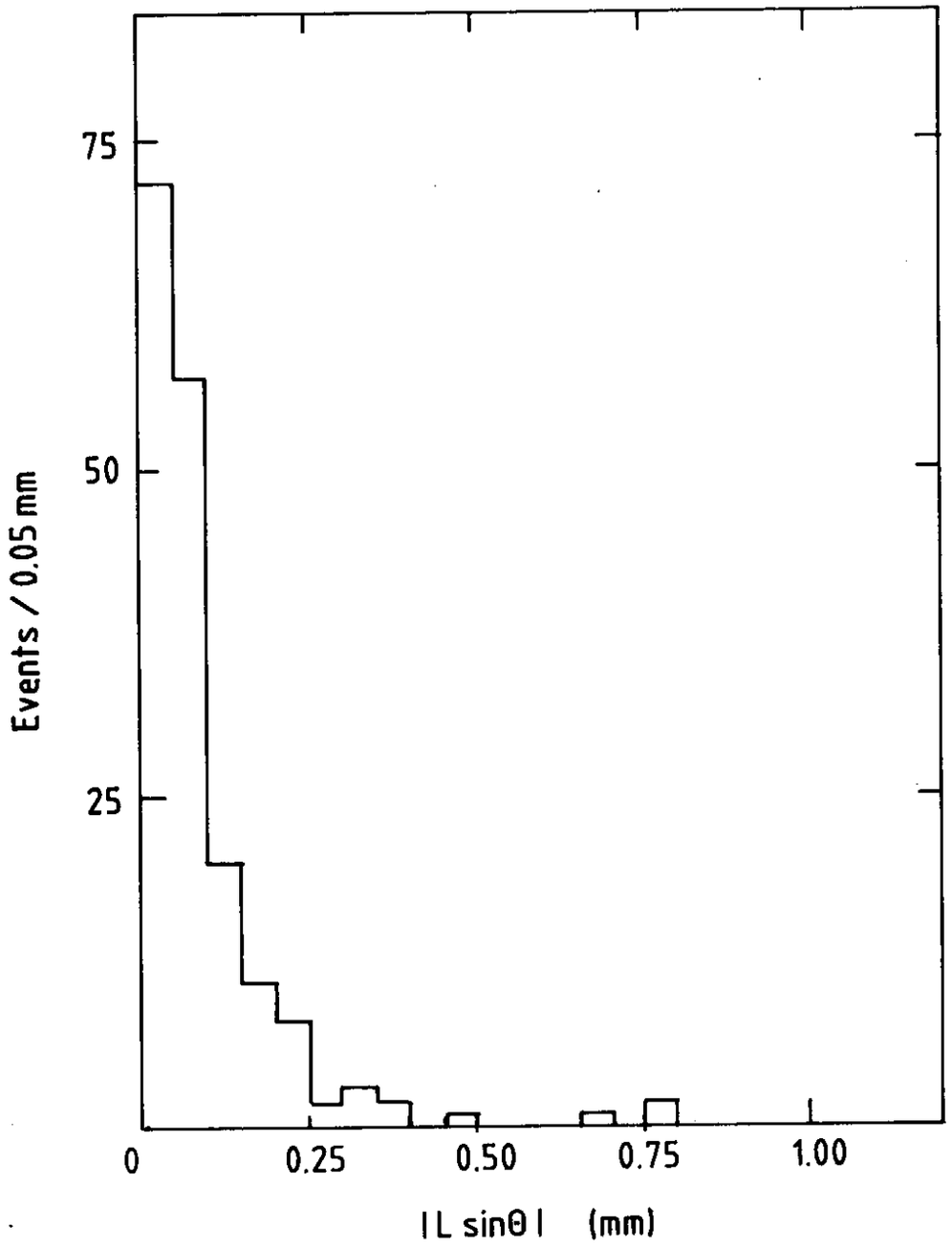

FIG. 7

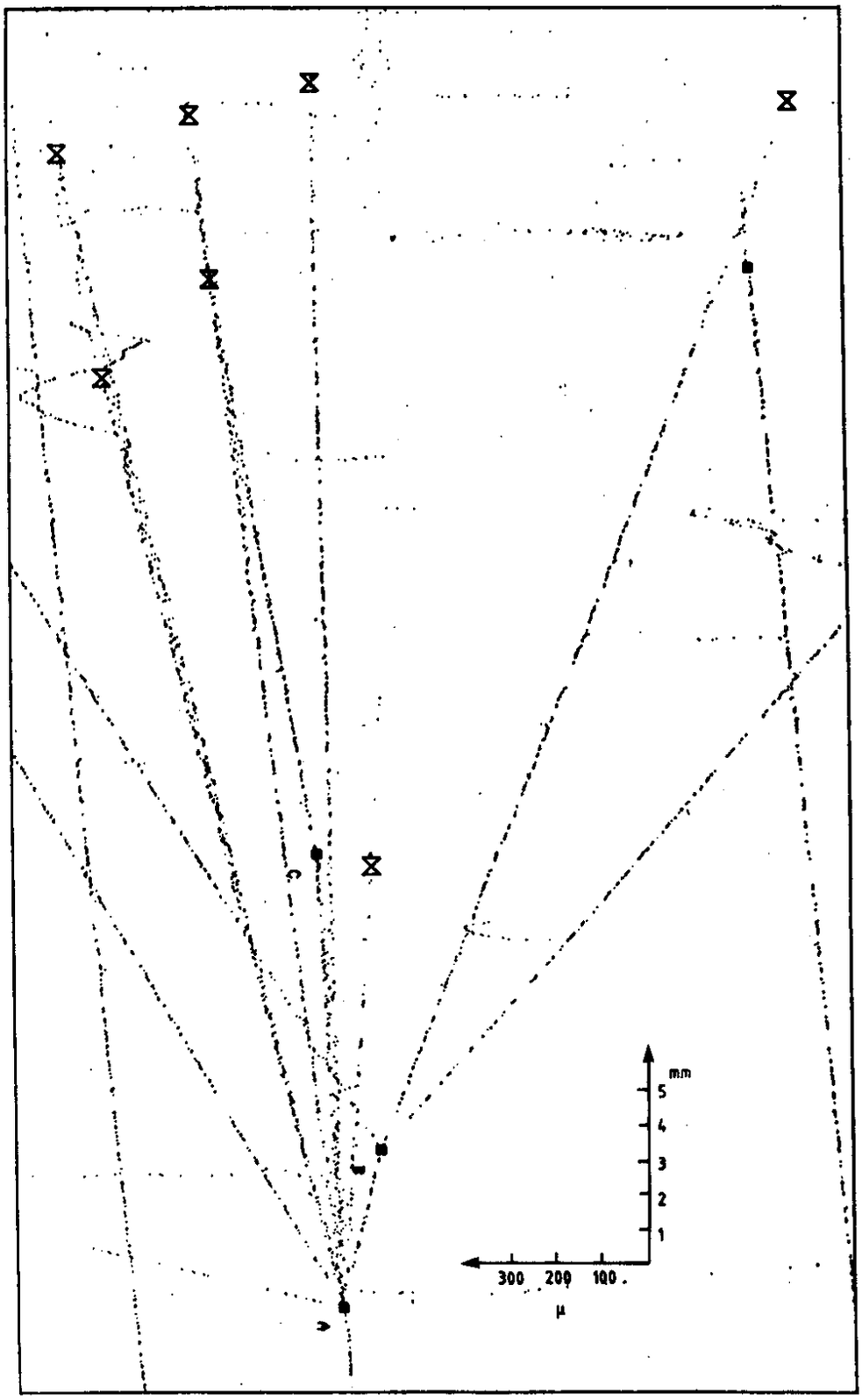

FIG. 8

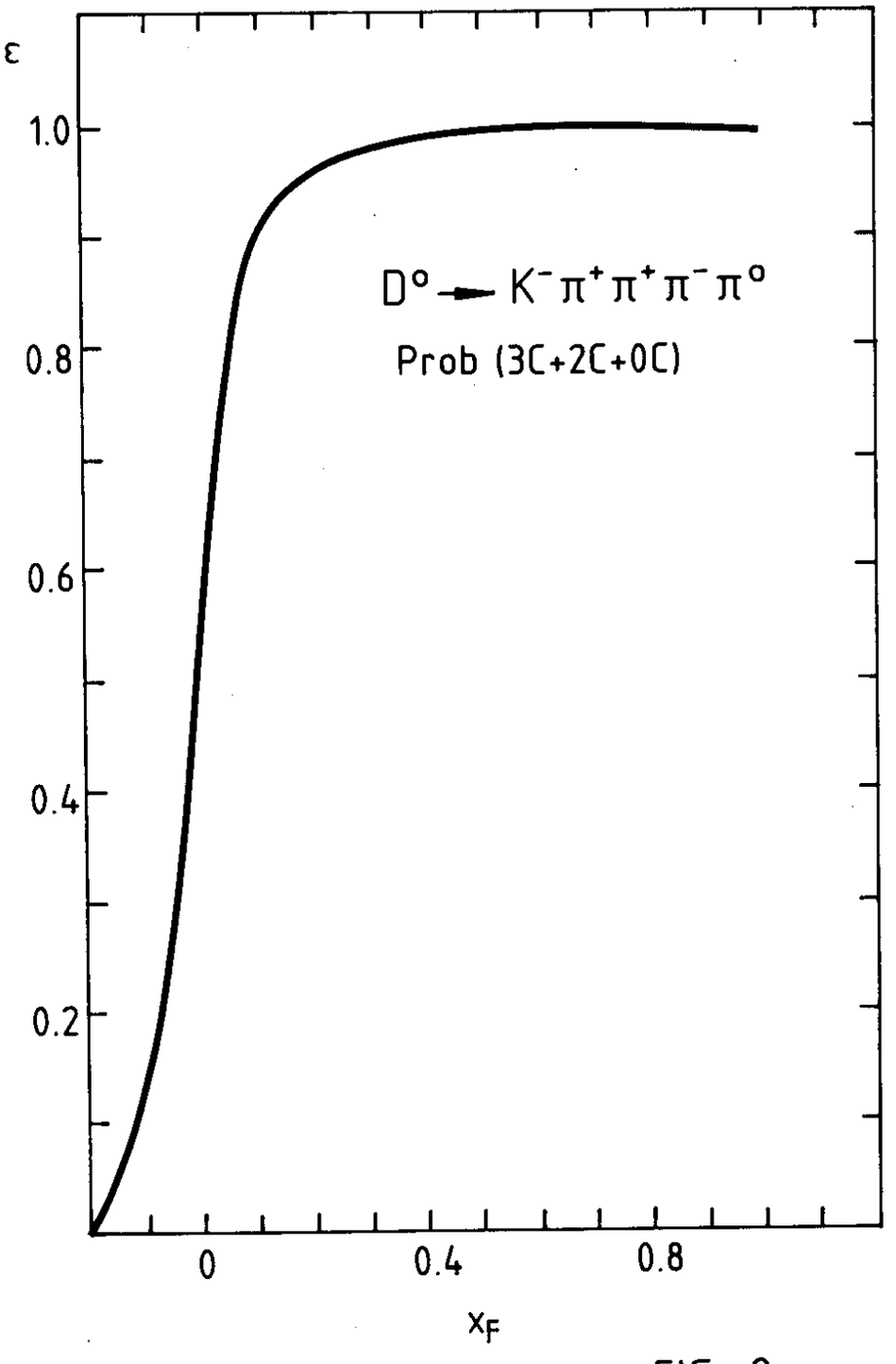

FIG. 9

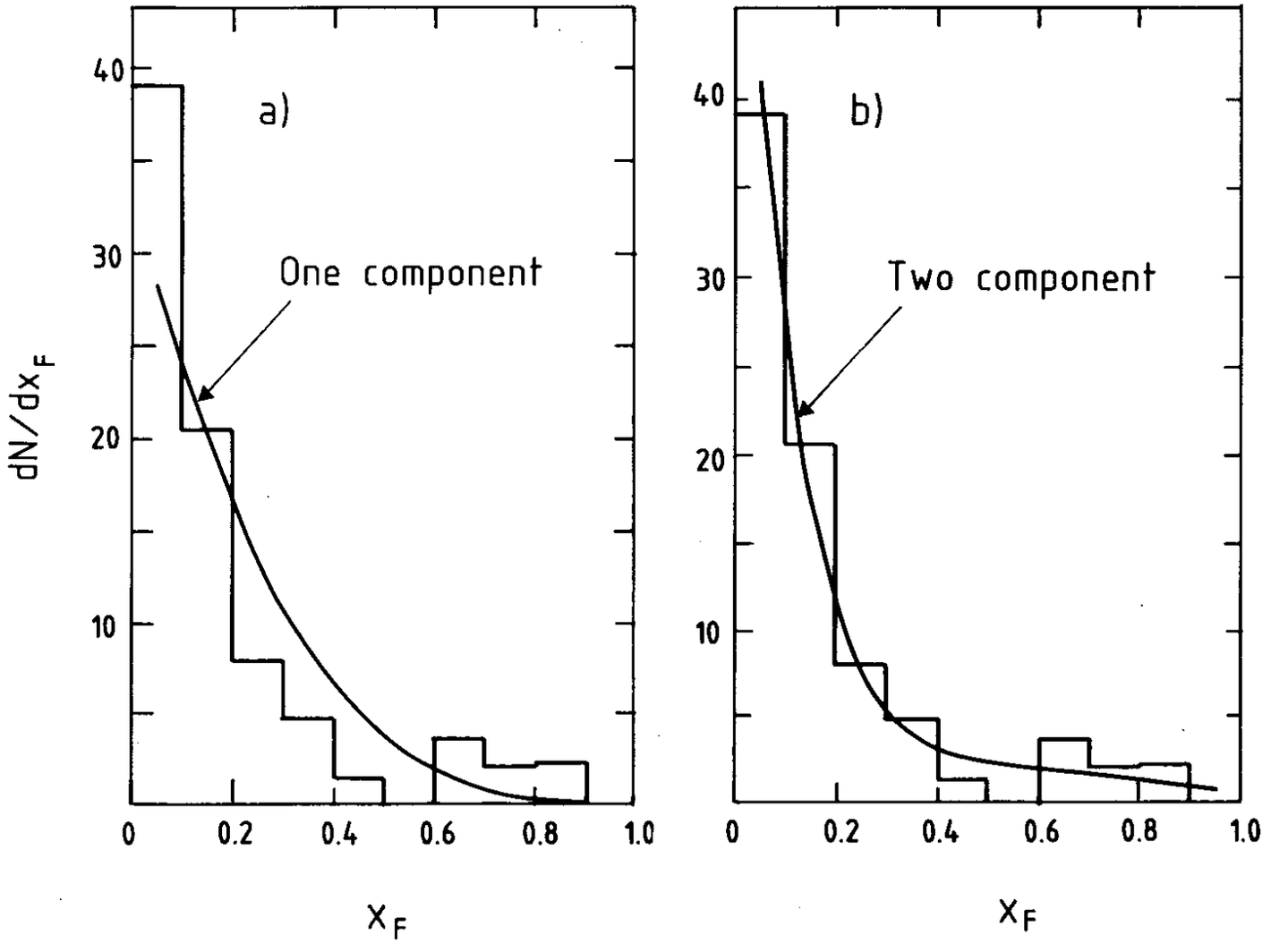
a)
One component
b)
Two component
dN/dx_F
x_F
x_F
40
30
20
10
0
0.2
0.4
0.6
0.8
1.0

FIG. 10

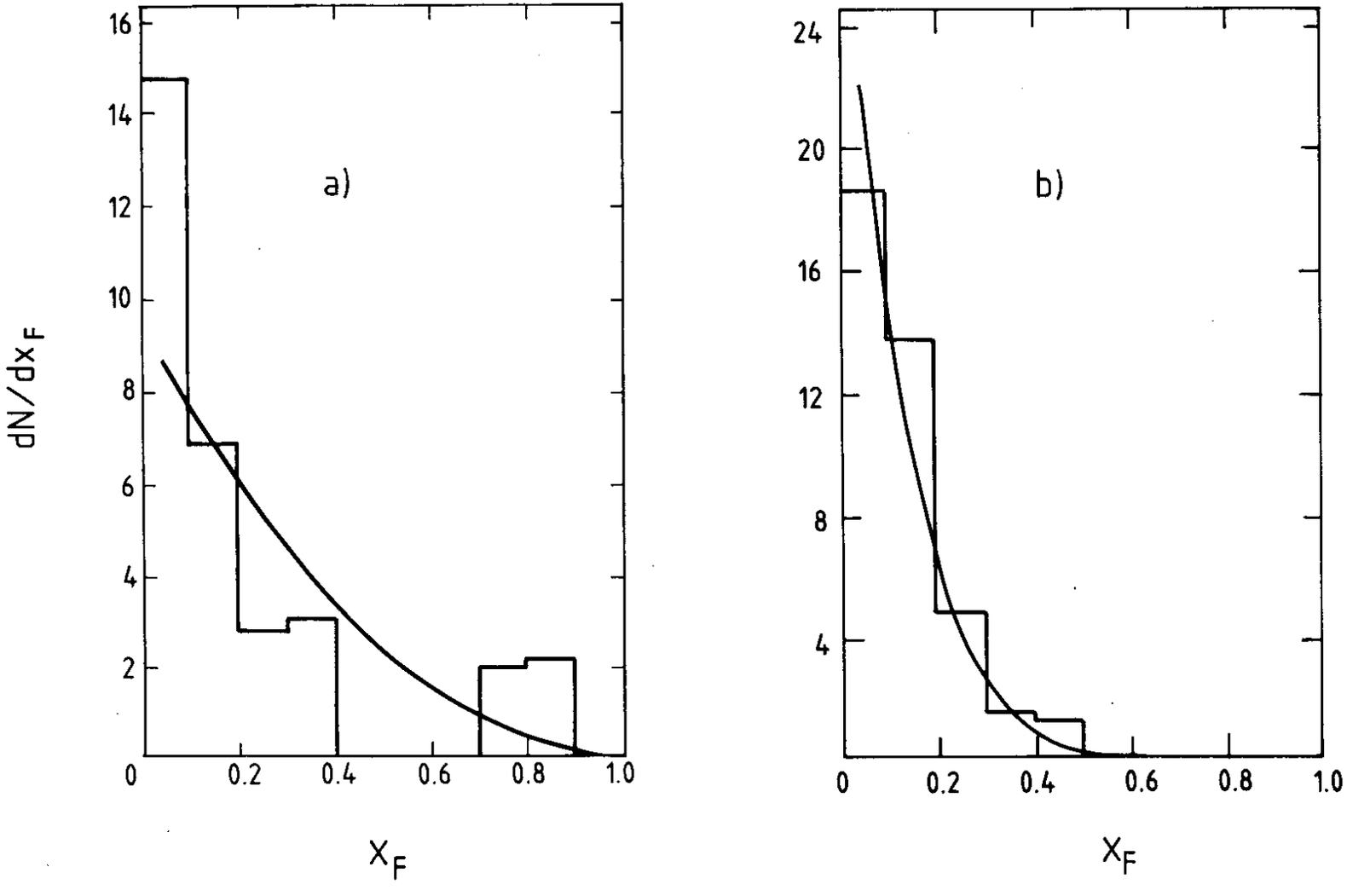

FIG. 11

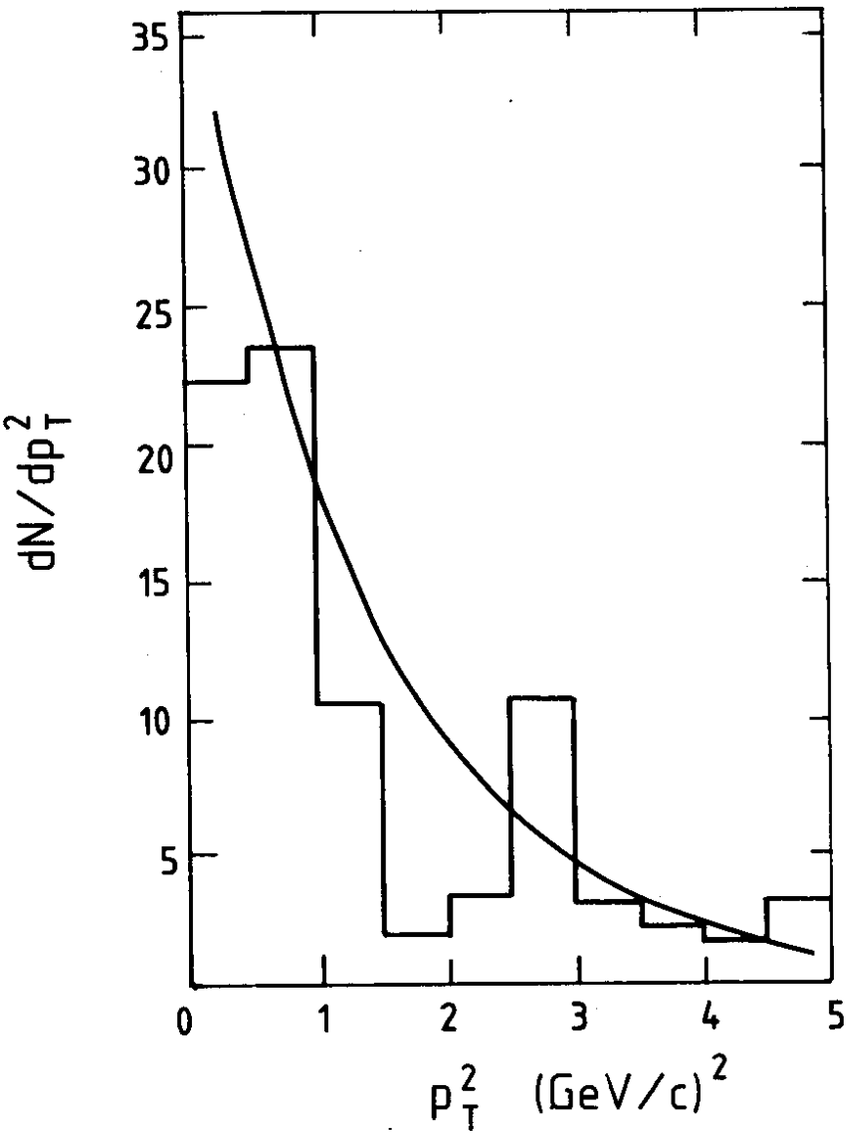

FIG. 12

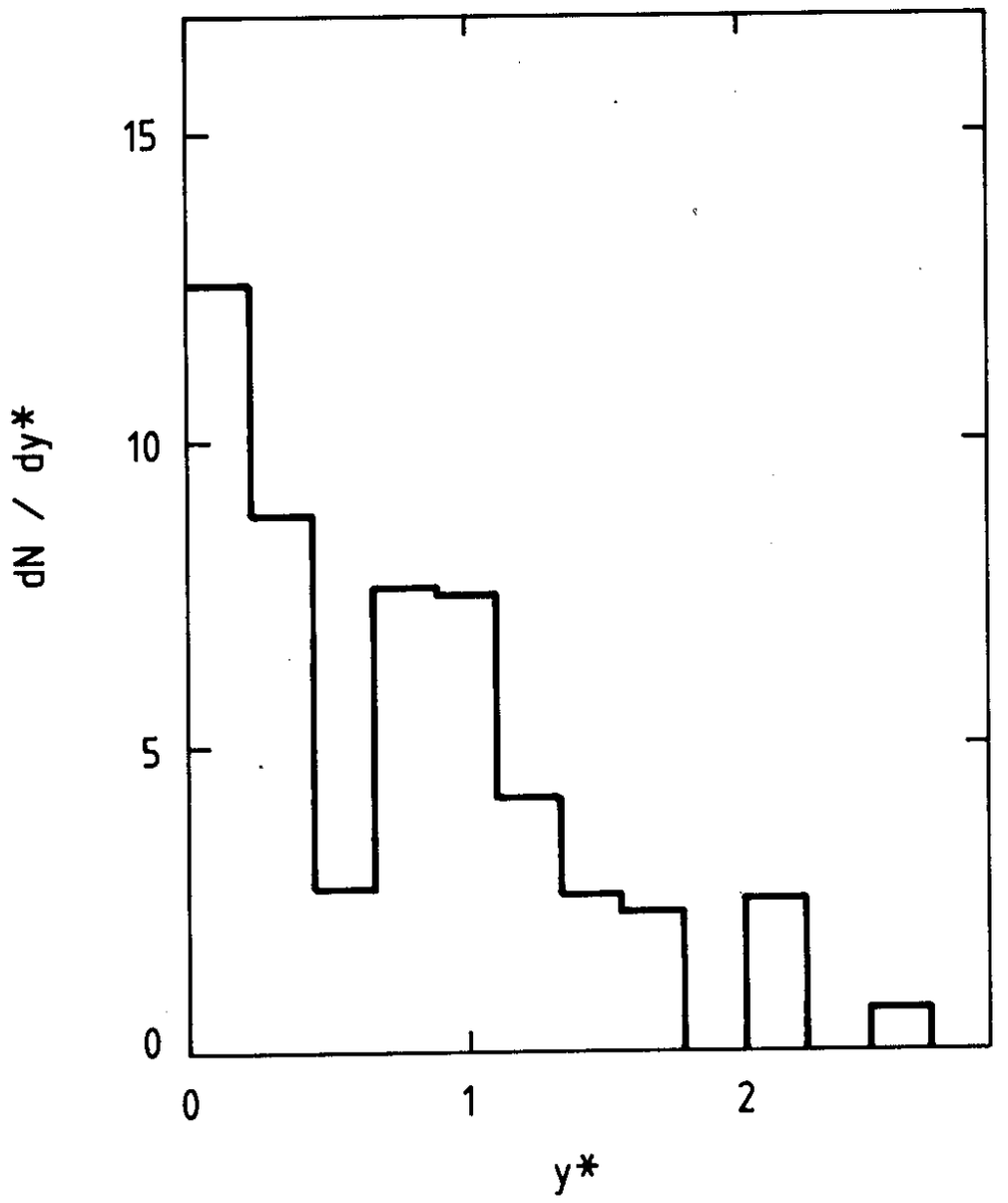

FIG. 13

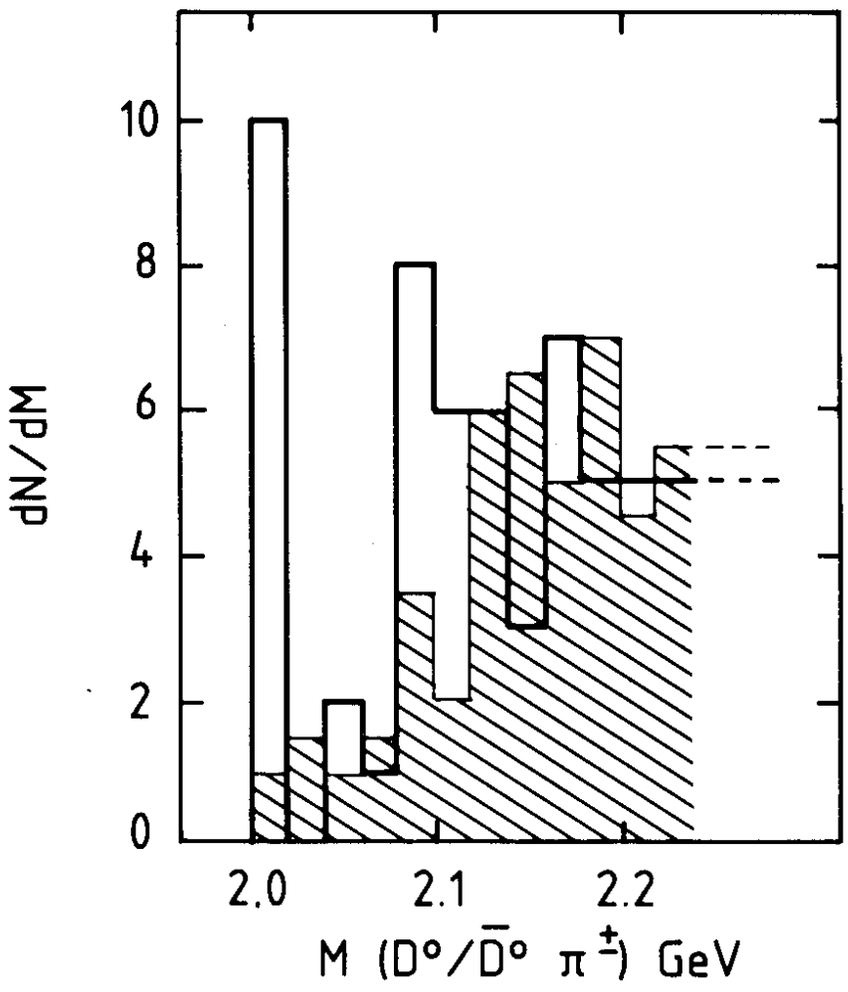

FIG. 14

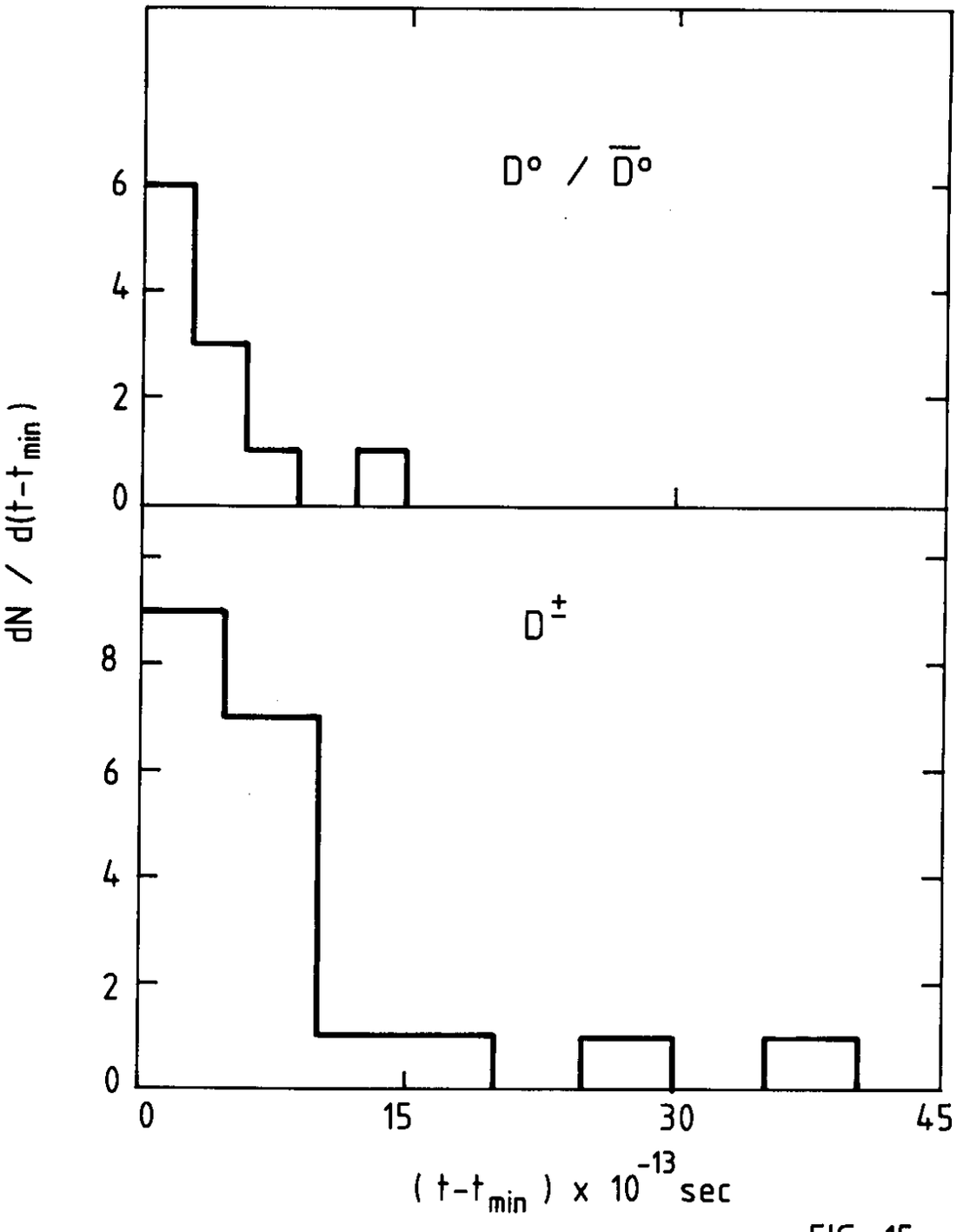
D° / $\overline{D}$°
$D^{\pm}$
6
4
2
0
8
6
4
2
0
0
15
30
45
dN / d(t-t_{min})
(t-t_{min}) x 10^{-13} sec

FIG. 15

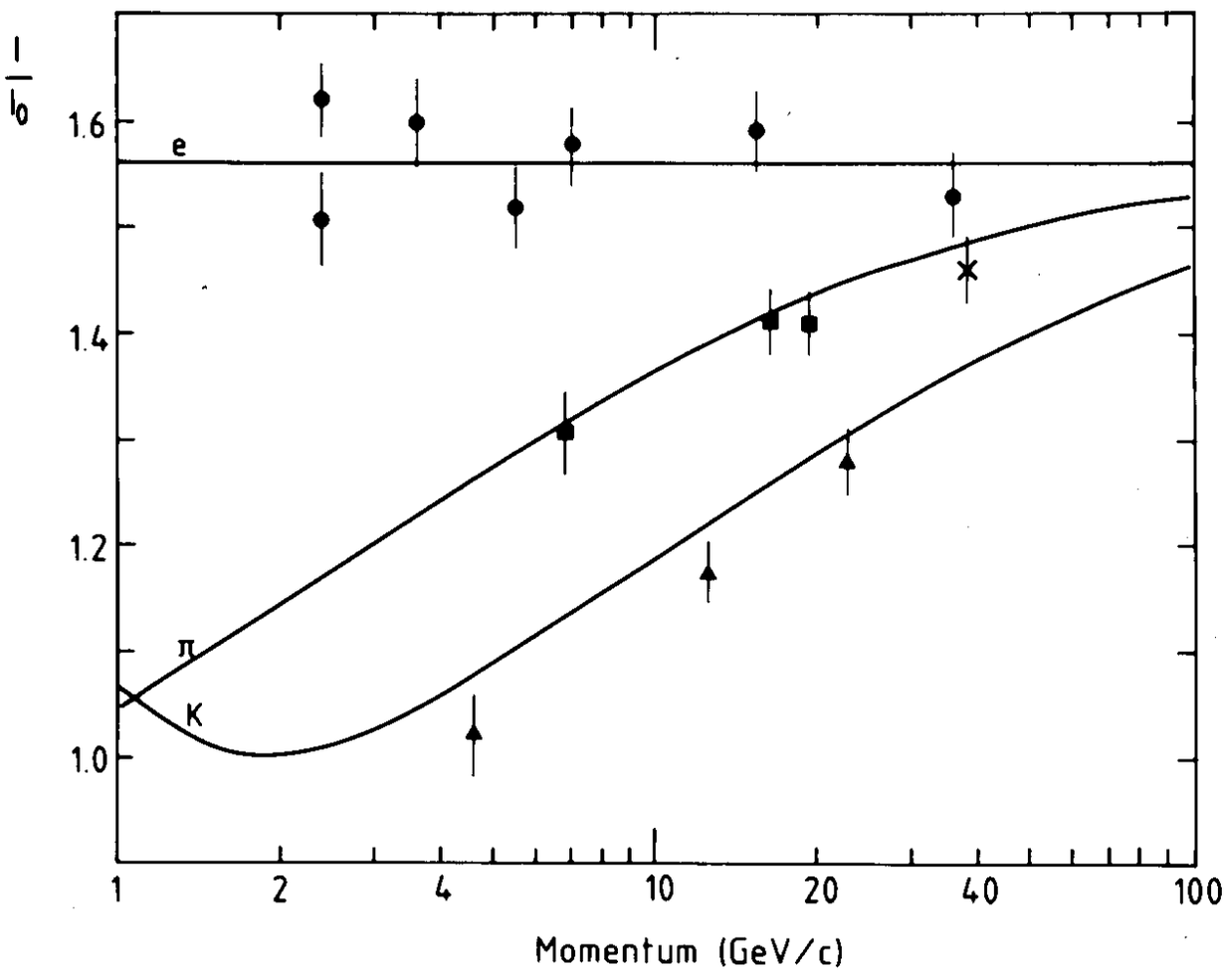

FIG. 16

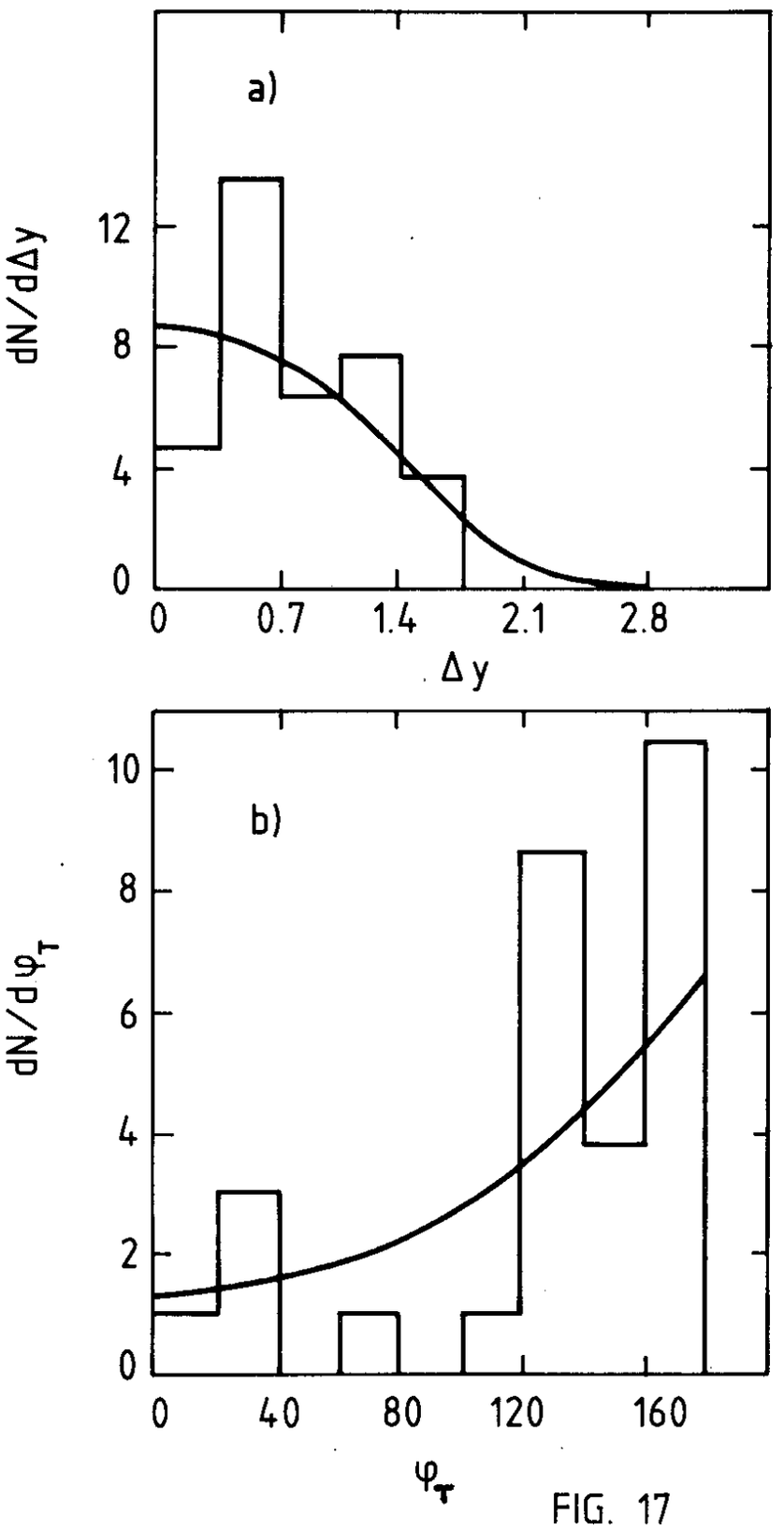

FIG. 17